Journal of Molecular Structure 1256 (2022) 132513

Contents lists available at ScienceDirect

Journal of Molecular Structure

journal homepage: www.elsevier.com/locate/molstr

Synthesis, spectroscopic, DFT calculations, biological activities and molecular docking studies of new isoxazolone, pyrazolone, triazine, triazole and amide derivatives

Kurls E. Anwer, Galal H. Sayed, Ramadan M. Ramadan*

Chemistry Department, Faculty of Science, Ain Shams University, Cairo, Egypt

ARTICLE INFO

Article history:
Received 1 December 2021
Revised 12 January 2022
Accepted 28 January 2022
Available online 30 January 2022

Keywords:
Heterocyclic compounds
NMR spectra
DFT studies
Antimicrobial activity
Cytotoxicity screening
Molecular docking

ABSTRACT

Ethyl-2-cyano-2-(2-(3-nitrophenyl)hydrazono)acetate was synthesized and used as a versatile reagent for the synthesis of different heterocyclic compounds such as isoxazolone, pyrazolone, triazine, triazole and amide derivatives via its reactions with different nucleophiles. Conventional, microwave and grinding techniques were used for synthesis of the newly isolated derivatives. Various physical parameters were calculated from the percentage yield and reaction time in order to compare between the three techniques. The reported compounds were characterized by elemental analyses and different spectroscopic tools such as IR, ^{1}H NMR, ^{13}C NMR and mass spectrometry. The optimized molecular geometries of some selected compounds were investigated using the density functional theory (DFT/B3LYP) method with the use of double zeta plus polarization basis set 6–31 G (d,p) for the C, H, N, O and S atoms. The quantum global reactivity descriptors were also calculated and discussed. The antibacterial and cytotoxicity screening of those compounds were performed to determine their therapeutic potential. Molecular docking of the compounds was also examined. The different biological studies as well as the molecular docking were correlated to each other, and supported that the compounds could bind to DNA, possibly, via intercalative mode and showed a various DNA binding potency.

1. Introduction

Azo dyes are the most important synthetic coloring reagents widely used in industry for textile, printing and paper manufacturing [1]. Azo compounds have harmful effects on humans and aquatic environment and there are urgent demands for the elimination of them or convert them into useful and safe products. However recently, azo dyes showed broad biological activities such as: anti-inflammatory, acaricidal, analgesic, anthelmintic, antagonist, antiviral, antioxidant, herbicidal, anticancer, antimitotic, insecticidal and antimicrobial activities [2–12]. On the other hand, synthetic heterocyclic compounds, such as nitrogen containing heterocycles, have proved to have diverse and significant therapeutic potential. Interest in these derivatives such as pyrazole, pyrazolone, triazine and triazole derivatives is stemmed from their promising applications in industry and biology [13–27].

Green chemistry approach is the science of design of chemical processes that reduce or eliminate the generation of hazardous compounds. It prevents pollution at the molecular level. The use of microwave irradiation and grinding techniques in syntheses of chemical compounds are also branches of the green chemistry processes. One-pot multicomponent organic reactions [28] have found to be an efficient tool for benign synthesis with the effectiveness for their productivity, facile execution and generation of highly diverse products from easily available starting materials in a single operation. Therefore, such technique has drawn much more attention because of its environmentally safe, more convenient, and rapid synthetic procedures that are highly desirable energy efficient. Compared with the conventional methods, microwave irradiation and grinding methods are much more environmentally tolerant and easily controlled. As an advantage, many organic reactions have been carried out in higher yield, shorter reaction time, and cleaner and milder conditions [29–31]. Thus, this type of green synthesis is now considered as significant process in organic chemistry because of its simplicity, mild conditions and economy. In this article, we report the reactions of ethyl-2-cyano-2-(2-(3-nitrophenyl)hydrazono)acetate derivative (**1**) with some selected amino derivatives. The reactions were carried out using conventional thermal technique along with using one pot microwave irradiation and grinding methods. Different isolated products were obtained with interesting structure features. Comparison between the consumed times and percentage yields, which resulting from

* Corresponding author.
E-mail address: r_m_ramadan@yahoo.com (R.M. Ramadan).

https://doi.org/10.1016/j.molstruc.2022.132513
0022-2860/

the three techniques was performed. The obtained derivatives were characterized by using different analytical and spectroscopic techniques.

2. Experimental

2.1. Reagents

All chemicals and reagents were of analytical reagent grade and purchased from Sigma Aldrich. All the solvents were purified according to the standard methods.

2.2. Instrumentation

Thin layer chromatography (TLC) was performed on pre-coated silica gel plates (Merck Kiesel gel $60F_{254}$, BDH). Melting points were determined on a digital Stuart SMP3 electric melting point apparatus and were uncorrected. Microwave reactor Anton Paar (monowave 300) was used for microwave irradiation reactions using borosilicate glass vials of 10 mL. IR measurements (cm^{-1}) were performed on a Perkin-Elmer 293 spectrophotometer using KBr disks. ^1H NMR and ^{13}C NMR spectra were recorded on a Varian Mercury 300 MHz spectrometer. Samples were dissolved in DMSO–d_6 with the use of TMS as an internal reference. Mass spectrometry measurements (EI, 70 eV) were carried out on a GC-2010 Shimadzu Gas chromatography mass spectrometer. Elemental microanalyses (CHN) were performed on a Perkin-Elmer CHN-2400 analyzer. The data were found to be in good agreement within ± 0.4% of the theoretical values.

2.3. Syntheses of the reported compounds

In the following sections, the synthesis of the starting reagent (thyl-2-cyano-2-(2-(3-nitrophenyl)hydrazono)acetate, **1**, will be given, followed by detail procedures for the reactions of **1** with some selected amino derivatives.

2.3.1. Ethyl-2-cyano-2-(2-(3-nitrophenyl)hydrazono)acetate (1)

3-Nitro aniline (1.38 g, 10 mmol) was dissolved in 10 mL of 50% aqueous HCl, and then cooled in an ice bath (5–10 °C). A cold aqueous solution of sodium nitrite (0.68 g, 10 mmol) was added dropwise with stirring. The formed diazonium salt was filtered into a cold solution of sodium acetate (4 g) and ethyl cyanoacetate (1.13 mL, 10 mmol) in ethanol (25 mL). The reaction mixture was stirred for 1 h. The product was recrystallized from ethanol to yield off-white crystals (m.p. 120–122 °C). $C_{11}H_{10}N_4O_4$ (262.22); Calcd.: C, 50.38; H, 3.84; N, 21.37. Found: C, 50.42; H, 3.79; N, 21.40. *m/z* 263 (P^+, 17.52%). IR (cm^{-1}): 3171 (υ_{NH}), 2222 ($\upsilon_{C\equiv N}$), 1741 ($\upsilon_{C=O}$), 1617 ($\upsilon_{C=N}$), 1532 (υas_{NO2}), 1352 (υs_{NO2}). ^1H NMR (300 MHz, DMSO–d_6) δ (ppm): 1.30 (t, 3H, $\underline{CH_3}CH_2$), 4.30 (q, 2H, $CH_3\underline{CH_2}$), 7.60–8.23 (m, 4H, Ar-H), 9.54 (s, 1H, NH, D_2O exchangeable). ^{13}C NMR (300 MHz, DMSO–d_6) δ (ppm): 14.0 (CH_3), 61.7 (CH_2), 102.7 (CH, Ar), 110.7 (C = N), 118.6 (CN), 119.3 (CH, Ar), 121.8 (CH, Ar), 122.1 (CH, Ar), 130.7 (C–NH), 148.3 (C–NO_2), and 159.3 (C = O).

2.3.2. 3-Amino-4-(2-(3-nitrophenyl)hydrazono)isoxazol-5(4H)-one (2)

A mixture of compound **1** (2.62 g, 10 mmol), hydroxylamine hydrochloride (0.69 mL, 10 mmol), and anhydrous potassium carbonate (1.38 g, 10 mmol) in ethanol (25 mL) was refluxed for 4 h. The solution was left to cool and the formed solid was collected by filtration. The residue was washed several times with ethanol and the recrystallized from hot methanol to give orange crystals (m.p. 180–182 °C). $C_9H_7N_5O_4$ (249.19); Calcd.: C, 43.38; H, 2.83; N, 28.11. Found: C, 43.44; H, 2.71; N, 28.03. *m/z* 250 (P^+, 19.94%). IR (cm^{-1}): 3520 (υs_{NH2}), 3429 (υas_{NH2}), 3287 (υ_{NH}), 1663 ($\upsilon_{C=O}$), 1600, 1579 ($\upsilon_{C=N}$), 1532 (υas_{NO2}), 1348 (υs_{NO2}). ^1H NMR (300 MHz, DMSO–d_6) δ (ppm): 6.17 (s, 2H, NH_2, D_2O exchangeable), 7.44–8.17 (m, 4H, Ar-H), 13.21 (s, 1H, NH, D_2O exchangeable). ^{13}C NMR (300 MHz, DMSO–d_6) δ (ppm): 109.8 (CH, Ar), 111.8 (CH, Ar), 117.8 (CH, Ar), 126.8 (CH, Ar), 130.4 (C = N), 145.6 (C–NH), 148.8 (C–NO_2), 156.1 (H_2N–C = N), 171.4 (C = O).

2.3.3. 5-Amino-4-(2-(3-nitrophenyl)hydrazono)–2,4-dihydro-3H-pyrazol-3-one (3)

Similar procedure was performed as used for **2** with the use of hydrazine hydrate (0.5 g, 10 mmol) to give brown crystals (m.p. 224–226 °C). $C_9H_8N_6O_3$ (248.20); Calcd.: C, 43.55; H, 3.25; N, 33.86. Found: C, 43.49; H, 3.07; N, 33.74. *m/z* 249 (P^+, 32.68%). IR (cm^{-1}): 3455 (υas_{NH2}), 3322 (υs_{NH2}), 3358 (υ_{NH}) 3201(υ_{NH}), 1676 ($\upsilon_{C=O}$), 1620, 1577 ($\upsilon_{C=N}$), 1534 (υas_{NO2}), 1352 (υs_{NO2}). ^1H NMR (300 MHz, DMSO–d_6) δ (ppm): 5.97 (s, 2H, NH_2, D_2O exchangeable), 7.49–8.41 (m, 4H, Ar-H), 9.42 (s, 1H, NH, D_2O exchangeable), 10.59 (s, 1H, NH, D_2O exchangeable). ^{13}C NMR (300 MHz, DMSO–d_6) δ (ppm): 109.6 (CH, Ar), 118.0 (CH, Ar), 121.6 (CH, Ar), 125.6 (CH, Ar), 130.6 (C = N), 143.7 (C–NH), 148.8 (C–NO_2), 149.9 (H_2N–C = N), 158.2 (C = O).

2.3.4. 5,5′-((1,4-Phenylenebis(methanylylidene))bis(azanylylidene))bis(4-(2-(3-nitrophenyl)hydrazono)–2,4-dihydro-3H-pyrazol-3-one) (4)

Similar procedure was performed as used for **2** with the use of terephthalaldehyde (1.34 g, 10 mmol) to give orange crystals (m.p. 268–270 °C). $C_{26}H_{18}N_{12}O_6$ (594.51); Calcd.: C, 52.53; H, 3.05; N, 28.27. Found: C, 52.40; H, 3.19; N, 28.33. *m/z* 595 (P^+, 7.74%). IR (cm^{-1}): 3298 (υ_{NH}), 1692 ($\upsilon_{C=O}$), 1599, 1575 ($\upsilon_{C=N}$), 1518 (υas_{NO2}), 1351 (υs_{NO2}). ^1H NMR (300 MHz, DMSO–d_6) δ (ppm): 6.75 −7.89 (m, 14H, Ar-H), 9.98 (s, 2H, 2NH, D_2O exchangeable), 10.46 (s, 2H, 2NH, D_2O exchangeable). ^{13}C NMR (300 MHz, DMSO–d_6) δ (ppm): 107.5 (CH, Ar), 108.3 (CH, Ar), 111.0 (CH, Ar), 111.7 (CH, Ar), 116.2 (CH, Ar), 116.6 (CH, Ar), 117.5 (CH, Ar), 118.5 (CH, Ar), 120.1 (CH, Ar), 120.4 (CH, Ar), 121.3 (CH, Ar), 123.8 (CH, Ar), 124.8 (C, Ar), 128.7 (C, Ar), 129.0 (C = N), 129.2 (C = N), 129.5 (C = N), 129.8 (C = N), 130.6 (C–NH), 130.8 (C–NH), 146.0 (2*C–NO_2), 148.4 (H_2N–C = N), 148.7 (H_2N–C = N), and 151.7 (2*C = O).

2.3.5. 5-Amino-4-(2-(3-nitrophenyl)hydrazono)–2-phenyl-2,4-dihydro-3H-pyrazol-3-one (5)

Similar procedure was used as for **2** with the use of phenyl hydrazine (1.08 ml, 10 mmol) to give gray crystals (m.p. 202–204 °C). $C_{15}H_{12}N_6O_3$ (324.30); Calcd.: C, 55.56; H, 3.73; N, 25.92. Found: C, 55.01; H, 3.79; N, 25.88. *m/z* 325 (P^+, 61.18%). IR (cm^{-1}): 3404 (υ_{NH}), 3319 (υas_{NH2}), 3167 (υs_{NH2}), 1662 ($\upsilon_{C=O}$), 1619, 1590 (C = N), 1527(υas_{NO2}), 1349 (υs_{NO2}). ^1H NMR (300 MHz, DMSO–d_6) δ (ppm): 5.95 (bs, 2H, NH_2, D_2O exchangeable), 7.55–8.24 (m, 9H, Ar-H), 12.35 (s, 1H, NH, D_2O exchangeable), 12.89 (s, 1H, NH, D_2O exchangeable). ^{13}C NMR (300 MHz, DMSO–d_6) δ (ppm): 106.2 (CH, Ar), 110.4 (CH, Ar), 110.7 (CH, Ar), 110.9 (CH, Ar), 115.2 (CH, Ar), 118.6 (CH, Ar), 119.3 (CH, Ar), 121.2 (CH, Ar), 122.2 (CH, Ar), 130.7 (C = N–N), 142.5 (C, Ar), 143.0 (C, Ar), 148.3 (C–NO_2), 159.8 (C = N), and 160.3 (C = O).

2.3.6. 5-Amino-2-(2,4-dinitrophenyl)–4-(2-(3-nitrophenyl)hydrazono)–2,4-dihydro-3H-pyrazol-3-one (6)

A mixture of **1** (2.62 g, 10 mmol) and 2,4-dinitrophenyl hydrazine (1.98 g, 10 mmol) in acetic acid (30 mL) was refluxed for 5 h.The solid formed after cooling was collected by filtration, washed with ethanol and recrystallized from acetic acid to give brown crystals (m.p. 266–268 °C). $C_{15}H_{10}N_8O_7$ (414.29); Calcd.: C, 43.49; H, 2.43; N, 27.05. Found: C, 43.55; H, 2.57; N, 26.89. *m/z* 415 (P^+, 52.82%). IR (cm^{-1}): 3337 (υs_{NH2}), 3147 (υas_{NH2}), 3115 (υ_{NH}), 1659 ($\upsilon_{C=O}$), 1617, 1586 ($\upsilon_{C=N}$), 1510 (υas_{NO2}), 1332 (υs_{NO2}). ^1H NMR (300 MHz, DMSO–d_6) δ (ppm): 7.21–8.80 (m, 7H, Ar-H), 9.98 (s,

1H, NH, D_2O exchangeable), 10.38 (s, 1H, NH, D_2O exchangeable). ^{13}C NMR (300 MHz, DMSO–d_6) δ (ppm): 110.4 (CH, Ar), 115.4 (CH, Ar), 122.9 (2*CH, Ar), 129.5 (2*CH, Ar), 129.9 (CH, Ar), 130.3 (C, Ar), 130.7 (C, Ar), 136.4 (C = N), 136.6 (C = N), 148.3 (C–NO_2), 148.5 (2*C–NO_2), and 169.1 (C = O).

2.3.7. 2-(3-Nitrophenyl)−5-oxo-3-thioxo-2,3,4,5-tetrahydro-1,2,4-triazine-6-carbonitrile (8)

A mixture of **1** (2.62 g, 10 mmol) and thiourea (0.76 g, 10 mmol.) in dioxane (30 mL) was refluxed for 6 h. After cooling, the reaction mixture was poured onto cold water, the solid formed was collected by filtration, washed with ethanol and recrystallized from ethanol to give orange crystal (m.p. 188–190 °C). $C_{10}H_5N_5O_3S$ (275.24); Calcd.: C, 43.64; H, 1.83; N, 25.44; S, 11.65. Found: C, 43.55; H, 1.91; N, 25.37; S, 11.77. *m/z* 276 (P^+, 33.79%). IR (cm^{-1}): 3272 (υ_{NH}), 2179 ($\upsilon_{C\equiv N}$), 1677 ($\upsilon_{C=O}$), 1605 ($\upsilon_{C=N}$), 1527 (υas_{NO2}), 1374 (υs_{NO2}), 1335 (C = S). ^1H NMR (300 MHz, DMSO–d_6) δ (ppm): 7.36–7.95 (m, 4H, Ar-H). ^{13}C NMR (300 MHz, DMSO–d_6) δ (ppm): 112.0 (CH, Ar), 118.7 (CN), 125.8 (CH, Ar), 129.1 (CH, Ar), 135.3 (CH, Ar), 136.1 (C, Ar), 145.2 (C–NO_2), 152.0 (C = N), 168.8 (C = O), and 185.2 (C = S).

2.3.8. 2-(3-Nitrophenyl)−5-oxo-4-phenyl-3-thioxo-2,3,4,5-tetrahydro-1,2,4-triazine-6-carbonitrile (10)

Similar procedure was performed as used for **8** with the use of to give yellow crystals (m.p. 236–238 °C). $C_{16}H_9N_5O_3S$ (351.34), Calcd.: C, 54.70; H, 2.58; N, 19.93; S, 9.13. Found: C, 54.84; H, 2.48; N, 20.08; S, 9.07. *m/z* 352 (P^+, 22.40%). IR (cm^{-1}): 2221 ($\upsilon_{C\equiv N}$), 1693 ($\upsilon_{C=O}$), 1527 (υas_{NO2}), 1345 (υs_{NO2}), 1311 ($\upsilon_{C=S}$). ^1H NMR (300 MHz, DMSO–d_6) δ (ppm): 7.32–8.33 (m, 9H, Ar-H). ^{13}C NMR (300 MHz, DMSO–d_6) δ (ppm): 110.5 (CH, Ar), 110.8 (CH, Ar), 111.1 (CH, Ar), 115.4 (CH, Ar), 118.7 (CN), 119.4 (CH, Ar), 121.9 (CH, Ar), 122.3 (CH, Ar), 130.9 (CH, Ar), 142.5 (CH, Ar), 143.4 (C, Ar), 148.4 (C–NO_2), 153.1 (C, Ar), 159.8 (C = N), 160.5 (C = O) and 175.7 (C = S).

2.3.9. 2-((3-Nitrophenyl)diazenyl)−2-(5-thioxo-2,5-dihydro-1H-1,2,4-triazol-3-yl)acetonitrile (13)

Similar procedure was performed as used for **8** with the use of thiosemicarbazide (0.91 g, 10 mmol) in ethanol to give orange crystals (m.p. 272–274 °C). $C_{10}H_7N_7O_2S$ (289.27); Calcd.: C, 41.52; H, 2.44; N, 33.89; S, 11.08. Found: C, 41.60; H, 2.37; N, 33.81; S, 11.21. *m/z* 290 (P^+, 7.79%). IR (cm^{-1}): 3258, 3180 (υ_{NH}), 2184 ($\upsilon_{C\equiv N}$), 1639 ($\upsilon_{C=N}$), 1445 (*N = N*), 1523 (υs_{NO2}), 1342 (υas_{NO2}), 1293 (C = S). ^1H NMR (300 MHz, DMSO–d_6) δ (ppm): 3.76 (s, 1H, CN<u>CH</u>C=N), 4.48 (s, 1H, NH, D_2O exchangeable), 7.21–8.00 (m, 4H, Ar-H), 8.58 (s, 1H, NH, D_2O exchangeable). ^{13}C NMR (300 MHz, DMSO–d_6) δ (ppm): 50.3 (CN–<u>CH</u>–C = N), 111.6 (CH, Ar), 116.7 (CN), 117.7 (CH, Ar), 126.7 (CH, Ar, 129.8 (CH, Ar), 148.6 (C–NO_2), 156.1 (C–*N = N*), 167.0 (C = N), and 181.0 (C = S).

2.3.10. 2-((3-Nitrophenyl)diazenyl)−2-(5-oxo-2,5-dihydro-1H-1,2,4-triazol-3-yl)acetonitrile (14)

Similar procedure was performed as used for **8** with the use of semicarbazide hydrochloride (1.11 g, 10 mmol.) and anhydrous potassium carbonate (1.38 g, 10 mmol) to give pale gray crystals (m.p. 202–204 °C). $C_{10}H_7N_7O_3$ (273.21); Calcd.: C, 43.96; H, 2.58; N, 35.89. Found: C, 43.88; H, 2.67; N, 35.93. *m/z* 273 (P^+, 56.24%). IR (cm^{-1}): 3225, 3193 (υ_{NH}), 2216 ($\upsilon_{C\equiv N}$), 1738 ($\upsilon_{C=O}$), 1600 ($\upsilon_{C=N}$), 1504 ($\upsilon_{N=N}$), 1525 (υs_{NO2}), 1332 (υas_{NO2}). ^1H NMR (300 MHz, DMSO–d_6) δ (ppm): 3.01 (s, 1H, CN<u>CH</u>C=N, 4.24 (s, 1H, NH, D_2O exchangeable), 7.26–8.38 (m, 4H, Ar-H), 8.83 (s, 1H, NH, D_2O exchangeable), 12.45 (s, 1H, OH, D_2O exchangeable). ^{13}C NMR (300 MHz, DMSO–d_6) δ (ppm): 51.9 (CN–<u>CH</u>–C = N), 110.9 (CH, Ar), 118.8 (CN), 121.9 (CH, Ar), 131.0 (CH, Ar), 143.0 (CH, Ar), 148.3 (C–NO_2), 157.7 (C–*N = N*), 160.4 (C = N), 162.4 (C = O).

2.3.11. General procedure for synthesis of compounds (15–19)

A solution of **1** (2.62 g, 10 mmol) and anhydrous potassium carbonate (1.38 g, 10 mmol) in ethanol (25 mL) was refluxed for 3–8 h with either *p*-aminoazobenzene (1.97 g, 10 mmol), 2-amino-3-hydroxypyridine (1.10 g, 10 mmol), 2-aminothiazole (1.00 g, 10 mmol), 3-amine-5-phenyl-1H-pyrazole (1.59 g, 10 mmol), or 4-aminoantipyrine (2.03 g, 10 mmol). The obtained solid was collected by filtration, washed with ethanol, and then recrystallized from methanol.

(a) 2-Cyano-2-((3-nitrophenyl)diazenyl)-N-(4-(phenyldiazenyl) phenyl)acetamide (15)

Yellow crystals (m.p. 180–182 °C). $C_{21}H_{15}N_7O_3$ (413.40); Calcd.: C, 61.02; H, 3.66; N, 23.71. Found: C, 60.89; H, 3.81; N, 23.69. *m/z* 414 (P^+, 41.87%). IR (cm^{-1}): 3166 (υ_{NH}), 2220 ($\upsilon_{C\equiv N}$), 1692 ($\upsilon_{C=O}$), 1527, 1468 ($\upsilon_{N=N}$). ^1H NMR (300 MHz, DMSO–d_6) δ (ppm): 3.72 (s, 1H, CN<u>CH</u>CO), 7.63–8.30 (m, 13H, Ar-H), 12.41 (s, 1H, NH, D_2O exchangeable), 12.92 (s, 1H, OH, D_2O exchangeable). ^{13}C NMR (300 MHz, DMSO–d_6) δ (ppm): 58.3 (CN<u>CH</u>CO), 105.9 (CH, Ar), 110.4 (2* CH, Ar), 110.8 (2* CH, Ar), 110.9 (2*CH, Ar), 118.7 (CN), 119.3 (2*CH, Ar), 121.8 (2* CH, Ar), 122.2 (2* CH, Ar), 130.8 (C, Ar), 142.6 (C, Ar), 143.1 (2*C–*N = N*), 148.4 (C–NO_2), 160.3 (C = O).

(b) 2-Cyano-N-(3-hydroxypyridin-2-yl)−2-((3-nitrophenyl) diazenyl)acetamide (16)

Black crystals (m.p. > 300 °C). $C_{14}H_{10}N_6O_4$ (326.27); Calcd.: C, 51.54; H, 3.09; N, 25.76. Found: C, 51.48; H, 3.18; N, 25.81. *m/z* 327 (P^+, 24.07%). IR (cm^{-1}): 3435 (υ_{NH}), 2222 ($\upsilon_{C\equiv N}$), 1696 ($\upsilon_{C=O}$), 1619, 1594 ($\upsilon_{C=N}$), 1524 ($\upsilon_{N=N}$). ^1H NMR (300 MHz, DMSO–d_6) δ (ppm): 3.82 (s, 1H, CN<u>CH</u>CO), 7.12–8.31 (m, 7H, Ar-H), 12.46 (bs, 4H, OH, D_2O exchangeable). ^{13}C NMR (300 MHz, DMSO–d_6) δ (ppm): 52.9 (CN<u>CH</u>CO), 104.7 (CH, Ar), 110.6 (CH, Ar), 110.8 (CH, Ar), 111.7 (CH, Ar), 118.5 (CN), 119.5 (CH, Ar), 122.3 (CH, Ar), 122.4 (CH, Ar), 130.8 (C, Ar), 144.5 (C–*N = N*), 148.4 (C–OH & C–NO_2), and 161.5 (C = O).

(c) 2-Cyano-2-((3-nitrophenyl)diazenyl)-N-(thiazol-2-yl)acetamide (17)

Gray crystals (m.p. 258–260 °C). $C_{12}H_8N_6O_3S$ (316.29); Calcd.: C, 45.57; H, 2.55; N, 26.57; S, 10.14. Found: C, 45.44; H, 2.67; N, 26.41; S, 10.22. *m/z* 317 (P^+, 38.52%). IR (cm^{-1}): 3176 (υ_{NH}), 2222 ($\upsilon_{C\equiv N}$), 1693 ($\upsilon_{C=O}$), 1619 ($\upsilon_{C=N}$), 1526 ($\upsilon_{N=N}$). ^1H NMR (300 MHz, DMSO–d_6) δ (ppm): 3.84 (s, 1H, CN<u>CH</u>CO), 7.00–8.33 (m, 6H, Ar-H), 12.54 (s, 1H, NH, D_2O exchangeable). ^{13}C NMR (300 MHz, DMSO–d_6) δ (ppm): 52.7 (CN<u>CH</u>CO), 110.4 (CH, Ar), 110.7 (CH, Ar), 111.0 (CH, Ar), 118.6 (CN), 119.3 (CH, Ar), 121.8 (CH, Ar), 122.1 (CH, Ar), 130.7 (C–NH), 143.2 (C–*N = N*), 148.3 (C–NO_2), and 160 (C = O).

(d) 2-Cyano-2-((3-nitrophenyl)diazenyl)-N-(3-phenyl-1H-pyrazol-5-yl)acetamide (18)

Yellow crystals (m.p. 170–172 °C). $C_{18}H_{13}N_7O_3$ (375.35); Calcd.: C, 57.60; H, 3.49; N, 26.12. Found: C, 57.49; H, 3.59; N, 25.99. *m/z* 376 (P^+, 21.95%). IR (cm^{-1}): 3299 (υ_{NH}), 2222 ($\upsilon_{C\equiv N}$), 1692 ($\upsilon_{C=O}$), 1599, 1575 ($\upsilon_{C=N}$), 1493 ($\upsilon_{N=N}$). ^1H NMR (300 MHz, DMSO–d_6) δ (ppm): 3.82 (s, 1H, CN<u>CH</u>CO), 5.81 (s, 1H, NH, D_2O exchangeable), 7.22–8.24 (m, 10H, Ar-H), 11.29 (s, 1H, OH, D_2O exchangeable). ^{13}C NMR (300 MHz, DMSO–d_6) δ (ppm): 52.4 (CN<u>CH</u>CO), 87.5 (CH, Py-H), 110.8 (CH, Ar), 112.0 (CH, Ar), 118.4 (CN), 112.5 (CH, Ar), 122.8 (CH, Ar), 124.4 (CH, Ar), 127.3 (CH, Ar), 128.6 (CH, Ar), 130.6 (CH, Ar), 130.8 (CH, Ar), 131.9 (C, Ar), 144.9 (C–NH), 145.4 (C–*N = N*), 148.4 (C–NO_2), 152.9 (C = N, Py), and 161.1 (C = O).

(e) 2-Cyano-N-(1,5-dimethyl-3-oxo-2-phenyl-2,3-dihydro-1H-pyrazol-4-yl)−2-((3-nitrophenyl)diazenyl)-acetamide (19)

Gray crystals (m.p. >300 °C). $C_{20}H_{17}N_7O_4$ (419.40); Calcd.: C, 57.28; H, 4.08; N, 23.38. Found: C, 57.37; H, 3.89; N, 23.26. *m/z* 420 (P^+, 13.09%). IR (cm^{-1}): 3168 (υ_{NH}), 2220 ($\upsilon_{C\equiv N}$), 1691 ($\upsilon_{C=O}$), 1617 ($\upsilon_{C=N}$), 1524 ($\upsilon_{N=N}$). ^1H NMR (300 MHz, DMSO–d_6) δ (ppm): 3.31 (s, 3H, Py-CH_3), 3.84 (s, 1H, CN<u>CH</u>CO), 3.88 (s, 3H, N–CH_3), 7.62–8.33 (m, 9H, Ar-H), 12.34 (s, 1H, NH, D_2O exchangeable). ^{13}C NMR (300 MHz, DMSO–d_6) δ (ppm): 10.9 (CH_3), 32.2 (N–CH_3), 52.9 (CN<u>CH</u>CO), 105.9 (C-Py), 110.5 (CH, Ar), 111.0 (CH, Ar), 118.7 (CN),

119.4 (CH, Ar), 121.8 (CH, Ar), 121.9 (2*CH, Ar), 122.3 (2*CH, Ar), 130.9 C-Py), 142.6 (CH, Ar), 143.1 (C–N = N), 148.4 (C–NO_2), 159.8 (C, Ar), 160.4 (C = O), and 160.9 (C = O).

2.4. Computational studies

All calculations were carried out using Gaussian 09 W software package [32] with DFT (B3LYP) method using double zeta plus polarization basis set 6–31 G (d,p) for C, H, N, O and S atoms.

2.5. Biological activity studies

2.5.1. Antimicrobial activity

Some selected compounds were tested *in vitro* for their antibacterial activities with the use of agar well diffusion method. Experimental details of the investigations are as described previously [33]. The antibacterial activity was screened against two bacterial strains (*E. coli* and *Bacillus subtilis*). Ampicillin used as standards for the antibacterial activity. The measurements were performed in triplicates for each compound, and their average values are reported.

2.5.2. Cytotoxicity screening

Human liver carcinoma cell line (HepG2) and breast cancer cell lines (MCF7) were used for *in vitro* screening experiments for some of the reported compounds. The cancer cells were obtained frozen in liquid nitrogen (−180 °C) from the American Type Culture Collection. The tumor cell lines were maintained in the National Cancer Institute, Cairo, Egypt, by serial sub-culturing. Cell culture cytotoxicity assays were carried out as described in literature [34]. The experimental procedure of the investigations are as described previously [35]. The sensitivity of the human tumor cell lines to thymoquinone was determined by the SRB assay. The percentage of cell survival was calculated as follows:

Survival fraction = OD (treated cells) / OD (control cells)

The IC_{50} value is the concentration of thymoquinone required to produce 50% inhibition of cell growth. The results are compared with a similar run of Doxorubicin as an antitumor drug.

2.6. Molecular docking of compounds

The docking studies were performed using Molecular Operating Environment (MOE) package version 2014.0901. X-ray crystal structure of a B-DNA dodecamer d(CGCGAATTCGCG)2 running 30–50 direction (PDB ID: 1BNA) at 1.9 Å resolution. The DNA structure was opened in MOE, hydrogen atoms were inserted and subsequently energy optimization was carried out. The resulting model afforded to systematic conformational research with RMS gradient of 0.01 kcal/mol^{-1} using default parameters in the Site Finder tool implicated in MOE software.

3. Results and discussion

3.1. Stereochemistry and chemical reactivity prediction

The stereochemistry of some representative compounds namely, **1, 2, 3, 8, 13** and **17** were investigated by the hybrid density functional theory (DFT/B3LYP) using Gaussian 09 W software [32]. The structural coordinates were optimized in gas phase and double-zeta plus polarization basis set 6–31 G (d,p). In quantum chemistry, the two frontier orbitals HOMO and LUMO, in the molecular orbital diagram of a chemical compound, have remarkable contribution where they play important role in predicting the electric and optical properties of a molecule and the interaction with other species. They are also responsible for producing of the various charge transfer systems [36–38]. In order to investigate the most stable configuration of the compounds, It was focused first on the orientation of their functional groups with respect to each other and with respect to either the central NH–N or N = N moiety. The energetically stable model of compound **1** with a minimization energy of 18.79 kcal/mol showed specific features, where the molecule is almost planar. For example, the dihedral angles of N5-N6-C1-C2, N5-N6-C7-C8 and C1-O4-C15-C16 have 180° (Table 1, Fig. 1**a**). The bond angles (C2-N5-N6 = 120.9°, C7-N5-N6 = 120.7° and C1-C2-O3 = 122.4°) and bond lengths (N5-N6 = 1.33 Å, N5-C2 = 1.32 Å, C1-O3 = 1.24 Å and C13-N14 = 1.18 Å) were found to be in the reported normal range [39–41]. Notably, the C2-C13 bond has partial π-bond character due to the possible conjugation in the molecule. Fig. 1**b** shows the 2-D contour surface of the highest occupied molecular orbital (HOMO) and the lowest unoccupied molecular orbital (LUMO) as well as the charge distribution on the different atoms of compound **1**. The charge distribution showed that C2 and C13 involved in the cyano group has reasonable positive charges (0.175 and 0.061), which made it susceptible for nucleophilic attack. In addition, the oxygen atom of the O–C_2H_5 moiety has the highest negative charge (−0.503) relative to the other oxygen atoms in the molecule, which could facilitate elimination of an ethanol molecule during the reported reactions.

The optimized structure of **2** has a minimum energy = 19.49 kcal/mol. The structure is almost planar (the dihedral angles of N16-C1-C6-C5, C2-C1-N16-O17 and N7-N8-C9-C10 have the range 172.4–179.9°). Also, the bond angles N7-N8-C9 and C5-N7-N8 have approximately 120° (Table 1). In addition, the bond distances of N7-N8, N8-C9 and C10-O15 have similar values as shown in **1** (1.33, 1.31 and 1.22 Å, respectively). On the other hand, the bond length between C10 and the amino group (N15) was found to be 1.22 Å. As can be seen from Fig. 2, the NH proton performed intramolecular hydrogen bonding with the adjacent nitrogen and has a distance of 2.04 Å. The NH_2 group also formed hydrogen bond with the nitrogen atom of the isoxazolone ring. These finding are consistent with the signal broadening of both NH and NH_2 observed in the ^{1}H NMR spectrum of **2**. The minimized structure of compound **3** showed similar structure features like compound **2**. The minimization energy was found to be 4.72 kcal/mol. This value is much less than that of **2**, which could be due the extra hydrogen bond between the NH of the pyrazolone and the adjacent carbonyl oxygen. The three hydrogen bond distances (H25-N13, H23-N8, H24-O15) are 2.6, 2.0 and 2.7 Å, respectively (Table 1, Fig. 2). It also accounts with the signal broadening of the two NH signals in its ^{1}H NMR spectrum.

Optimization of the structure of compound **8** to the minimum energy (37.37 kcal/mol) gave a non-planar structure, Fig. 2. The two planes containing the nitrophenyl and the triazine moieties were perpendicular to each other (dihedral angle of C8-S14-C3-C4 equals to 89.2°). In addition, the torsion angles of C8-S14-N7-C4 and C8-N7-C3-C4 were 55.5 and 66.5°, respectively. On the other hand, the bond distance in the cyano group (C15-N16) was found to be equal to that of compound **1** (Table 1). The NH group formed intramolecular hydrogen bonding with the adjacent carbonyl oxygen with a separation of 2.52 Å, which is consistent with the spectroscopic findings. In case of compound **13**, the optimized structure (minimized energy = 29.34 kcal/mol) showed that the O_2N-Ph- and N = N–C- moieties are lying in one plane with dihedral angles approaches 180°. On the other hand, the two planes involving the triazole ring and the azo group were bent with dihedral angles about 130°, *i.e.*, the whole molecule is non-planar, Fig. 2. The bond angles around the azo and cyano groups ranged from 110 to 123° (for example, N7-N8-C9, C6-C5-N7, C9-C10-N11 and C10-C9-C19 were 112.1, 123.9, 121.4 and 112.5°, respectively). The bond length of the azo group (N7-N8) was 1.26 Å, which is in the normal range as reported previously [42,43]. In addition, the bond separation of the C = S group was similar to that of com-

Table 1
Selected bond lengths, bond angles and dihedral angles of the optimized structures by DFT calculations.

Compound	DFT data Bond length (Å)	Bond angle (°)	Dihedral angle (°)			
1	N5-N6	1.33	C2-N5-N6	120.9	N5-N6-C1-C2	180
	N5-C2	1.32	C7-N5-N6	120.7	N5-N6-C7-C8	180
	C1-O3	1.24	C1-C2-O3	122.4	C1-O4-C15-C16	180
	C13-N14	1.18				
2	N7-N8	1.33	N7-N8-C9	120.3	N16-C1-C6-C5	179.9
	N8-C9	1.31	C5-N7-N8	120.8	C2-C1-N16-	179.4
	C10-O15	1.22	C9-C11-N14	125.0	O17	172.4
	C10-N15	1.22	O17-N16-O18	124.1	N7-N8-C9-C10	
	H24-N13	2.04				
3	C5-N7	1.41	N7-N8-C9	119.3	C4-C5-N7-N8	176.5
	N8-C9	1.33	C5-N7-N8	120.8	N7-N8-C9-C10	174.0
	H25-N13	2.63	C11-C9-N8	131.4	C3-C4-C5-N7	179.8
	H23-N8	2.02				
	H24-O15	2.70				
8	C15-N16	1.22	C4-N7-N12	113.6	C8-S14-C3-C4	89.2
	C8-S14	1.71	N7-C8-S14	124.9	C8-S14-N7-C4	55.5
	C4-N7	1.45	N9-C10-O13	122.4	C8-N7-C3-C4	66.5
	O13-H24	2.53				
13	N7-N8	1.26	N7-N8-C9	112.1	C6-C5-N7-N8	178.4
	C13-S15	1.69	C6-C5-N7	123.9	N7-N8-C9-C19	105.6
	C9-N8	1.52	C9-C10-N11	121.4	C9-C10-N11-	25.13
	C5-N7	1.43	C10-C9-C19	112.5	H26	134.3
					N8-C9-C10-	
					N12	
17	N7-N8	1.27	N8-C9-C10	109.8	N7-N8-C9-C10	53.2
	C5-N7	1.43	C5-N7-N8	116.7	N7-N8-C9-C21	112.4
	N8-C9	1.50	C10-N11-H28	114.9	N8-C9-C10-	152.6
	N8-H28	2.14	C10-N11-C13		O12	

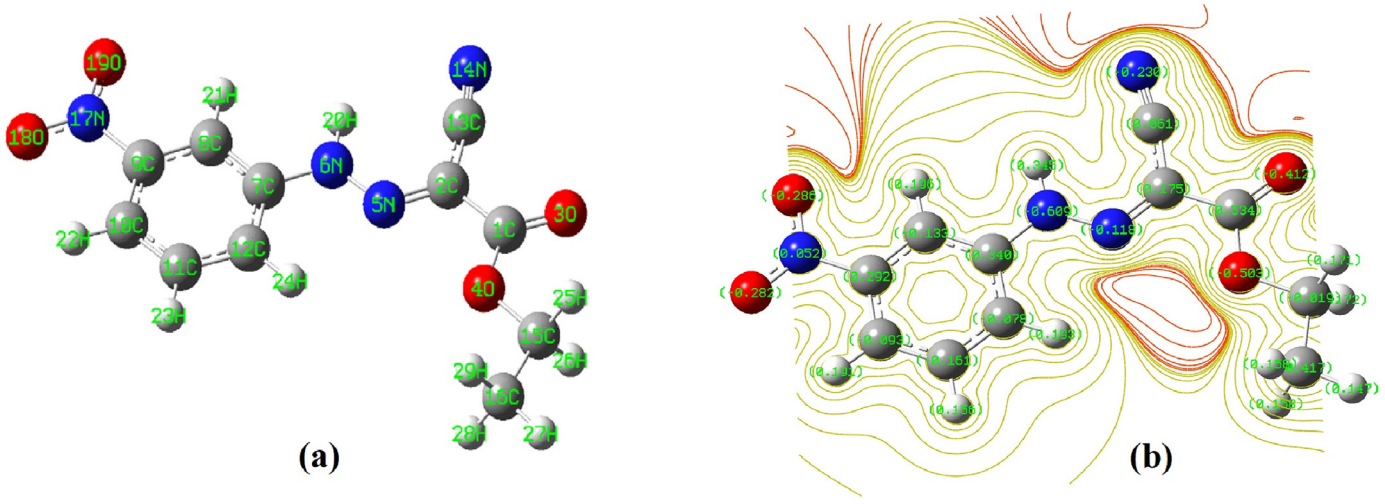

Fig. 1. (a) The optimized geometry of 1; (b) The 2-D contour surface of the HOMO and LUMO and the charge distribution on the atoms of 1.

pound **8** (1.70 Å). The optimized structure of compound **17** (minimized energy = 8.62 kcal/mol) displayed similar structure feature to that of **13**. That, the two moieties O_2N-Ph- and N = N–C- are in one plane with dihedral angles approximate 180°. However, the whole molecule is non-planar, where the two planes containing the nitrophenyl- and thiazolylacetamide- parts are bent (dihedral angles of N7-N8-C9-C10, N7-N8-C9-C21 and N8-C9-C10-O12 were 53.2, 112.4 and 152.6°, respectively). In addition, the bond angles around the azo group, such as N8-C9-C10 and C5-N7-N8, were 109.8 and 116.7°, respectively. Also, the bond angle C10-N11-H28 was 114.9°, which explained the direction of the NH proton towards the azo group to perform hydrogen bonding with N8 (NH…N = N distance = 2.14 Å). On the other hand, the bond lengths of the azo and cyano group were found to be similar to those found in the other compounds like **1, 8** and **13** (Table 1).

The global chemical reactivity parameters including HOMO, LUMO, energy gap (ΔE), electronegativity (X), chemical potential (V), electron affinity (A), ionization potential (I), chemical hardness (η), chemical softness (S) and electrophilicity (ω) of the investigated compounds are given in Table 2 [44]. The frontier molecular orbitals (HOMO and LUMO) energies were calculated by using the DFT method (B3LYP), where HOMO orbital energy demonstrates the electron donating ability and the LUMO orbital energy characterizes the electron withdrawing ability. The energy gap between the two frontier orbitals displays the molecular chemical stability, which it is a crucial parameter for determining molecular electrical transport properties. Smaller energy gaps reflect the easiness of the charge transfer (CT), and the polarization, which occurs within the molecules [45]. Notably, compound **13** has the smallest energy gap. In addition, the electronegativity factor is a reflection for the electrostatic potential, where the electron par-

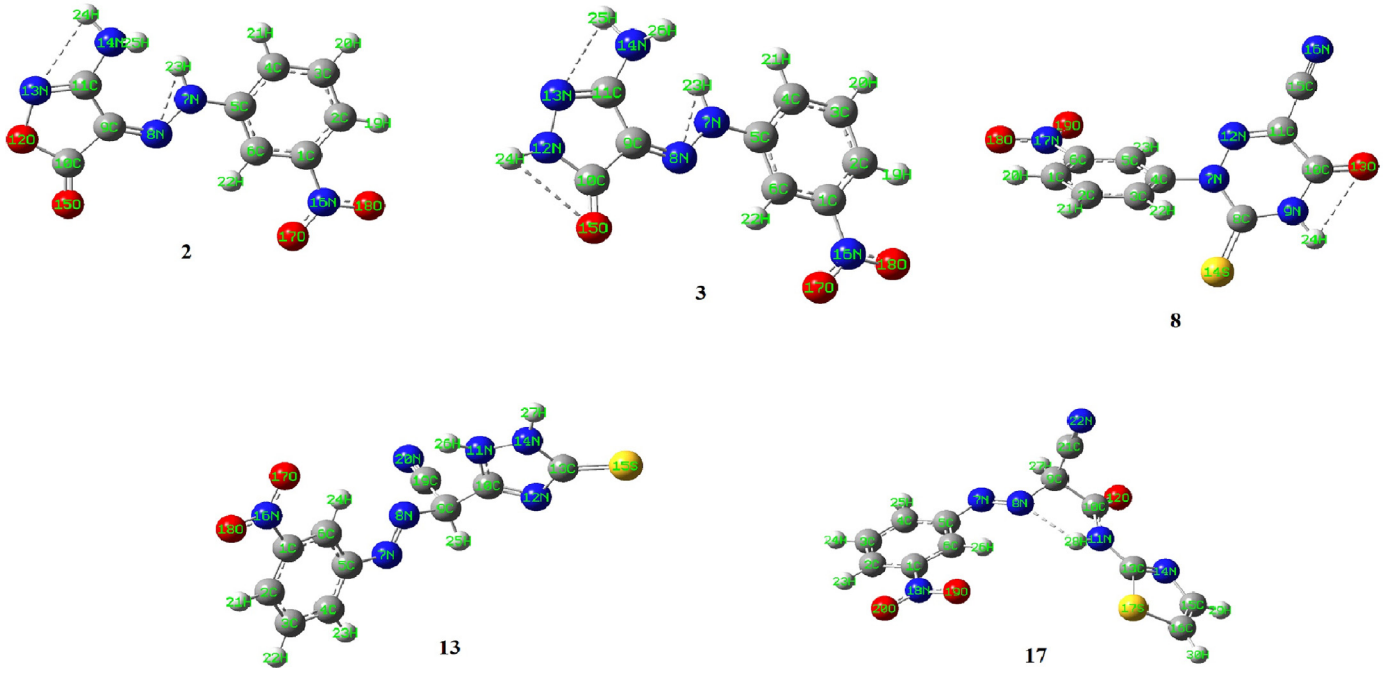

Fig. 2. The optimized geometries of the selected compounds.

Table 2
The global chemical reactivity descriptors for the investigated compounds.

Parameter	1	2	3	8	13	17
HOMO (eV)	−6.98	−6.85	−6.21	−7.17	−5.80	−7.32
LUMO (eV)	−3.28	−3.24	−2.95	−3.70	−3.70	−3.53
ΔE (eV)	3.70	3.61	3.27	3.47	2.10	3.79
X (eV)	5.13	5.04	4.58	5.43	4.75	5.43
V (eV)	−5.13	−5.04	−4.58	−5.43	−4.75	−5.43
A (eV)	3.28	3.24	2.95	3.70	3.70	3.53
I (eV)	6.98	6.85	6.21	7.17	5.80	7.32
η (eV)	1.85	1.80	1.63	1.73	1.05	1.90
S (eV)	0.93	0.90	0.82	0.87	0.53	0.95
ω (eV)	7.11	7.06	6.42	8.51	10.75	7.76

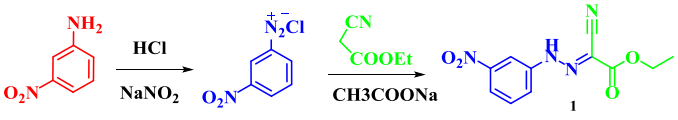

Scheme 1. Formation of ethyl-2-cyano-2-(2-(3-nitrophenyl)hydrazono)acetate, 1.

tially transferred from one of lower electronegativity to another of higher electronegativity. The order of decreasing electronegativity of the derivatives was found to be: **8** = **17** > **1** > **2** > **13** > **3**. Moreover, the results of small chemical hardness values for the reported derivatives reflect the ability of charge transfer within the molecule. The order of increasing the charge transfer within the molecule is: **17** > **1** > **2** > **8** > **3** > **13**.

3.2. Spectroscopic studies

The ethyl-2-cyano-2-(2-(3-nitrophenyl)hydrazono)acetate derivative (**1**) was synthesized through treatment of m-nitroaniline with sodium nitrile then coupled with ethyl cyanoacetate (Scheme 1). The mass spectrum of **1** exhibited a peak in its mass spectrum at m/z = 263 corresponding to the parent ion. The IR spectrum of **1** showed characteristic bands due to the NH, C≡N, C = O, C = N, and NO_2 functional groups (Fig. 3). In addition, the ^{1}H and ^{13}C NMR spectra of **1** were consistent with the given structure (Figs. 4 and 5). Interestingly, the signal due NH in the ^{1}H NMR spectrum appeared as a broad singlet at 9.54 ppm and disappeared on the addition of D_2O (Fig. 4).

Reaction of **1** with hydroxylamine hydrochloride in ethanol in presences of anhydrous potassium carbonate afforded the 3-amino-5-isoxazolone, **2**, (Scheme 2). The derivative was formed through nucleophilic attack of the amino group of the hydroxylamine on the cyanide group of **1**, followed by cyclization and elimination of an ethanol molecule. The IR spectrum of **2** (**Fig. S5**) showed characteristic bands due to the NH_2 and NH groups at 3520, 3475 and 3287 cm^{-1} with the disappearance of the C≡N group of **1**. In addition, the IR spectrum showed that the C = O band was shifted to lower wavenumber (1663 cm^{-1}). The ^{1}H NMR spectrum of **2** (**Figs. S6** and **S7**) displayed two distinct broad signals at 13.21 and 6.17 ppm due to NH and NH_2 protons, respectively. This broadening could be due to hydrogen bonding between the NH or NH_2 protons and adjacent nitrogen atoms. On the other hand, reaction of **1** with some selected amino derivatives (such as hydrazine hydrate, phenyl hydrazine and 2,4-dinitrophenyl hydrazine) yielded the pyrazolone derivatives **3, 5, 6** (Scheme 2). Similar to compound **2**, the reactions proceeded first with nucleophilic attack of the amino group of reagents on the cyano group of **1**, followed by formation of a pyrazolone ring with the removal of one molecule of ethanol. The structure of **3** was confirmed from its ^{1}H NMR spectrum (**Figs. S10** and **S11**). It displayed two very broad signals at 10.59 and 9.42 ppm due two different NH groups with the possibility of H-bond formation. The latter signal is probably due to the proton of NH of pyrazolone ring. The spectrum also displayed a singlet at 5.97 ppm, which is corresponding to the NH_2 moiety. In addition, the structure of **3** was further supported by carrying out its reaction with terephthalaldehyde in 2:1 ratio, where it afforded the corresponding bis-pyrazolone derivative **4** (Scheme 2). The mass spectrum of **4** showed a molecular ion peak at m/z = 595 [P^+] (7.74%). Furthermore, the ^{1}H NMR spectrum of **4** displayed two singlets at 10.46 and 9.98 ppm due to the NH groups. These signals disappeared from the spectrum when D_2O was added to solution.

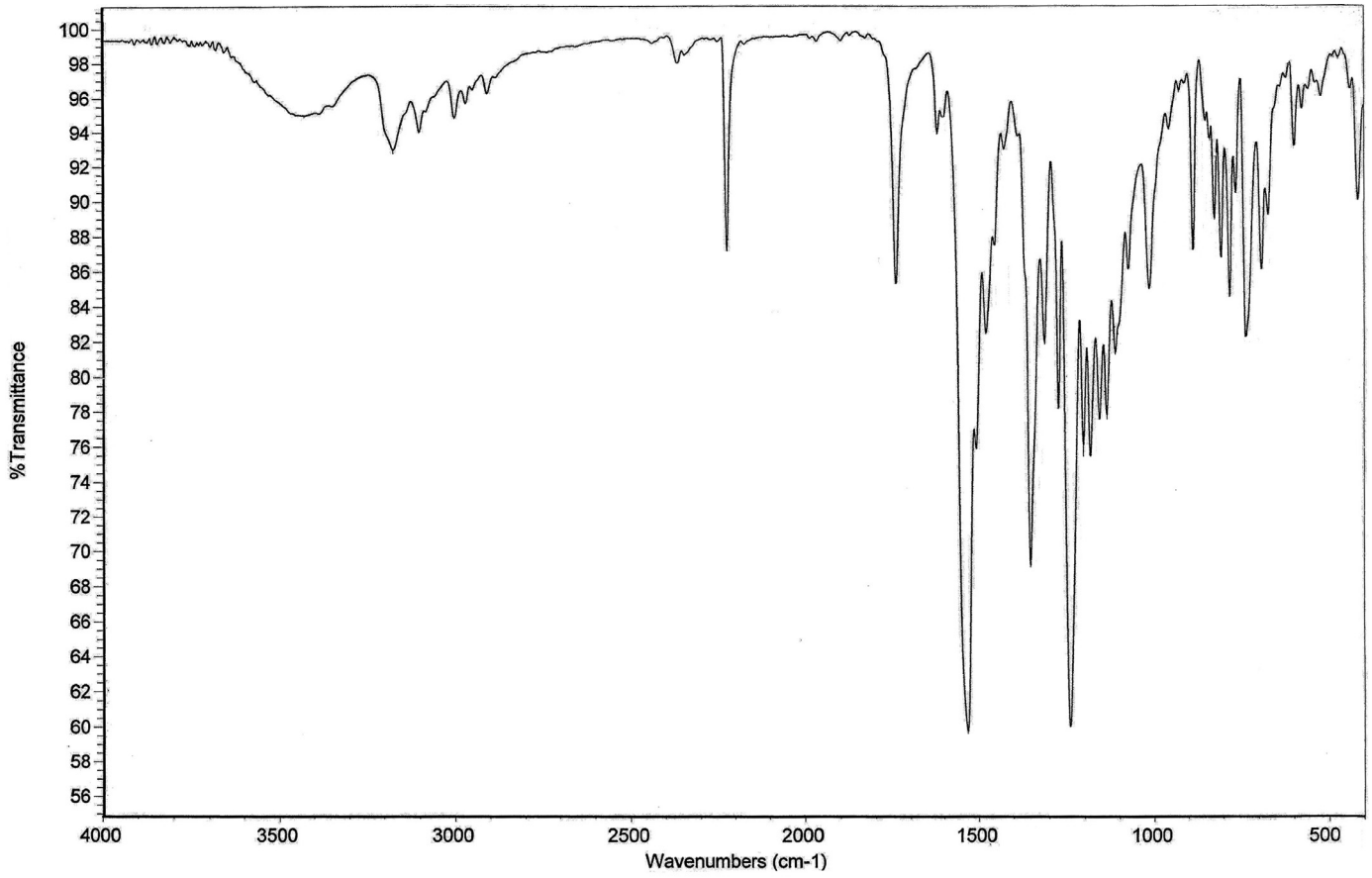

Fig. 3. IR spectrum of 1.

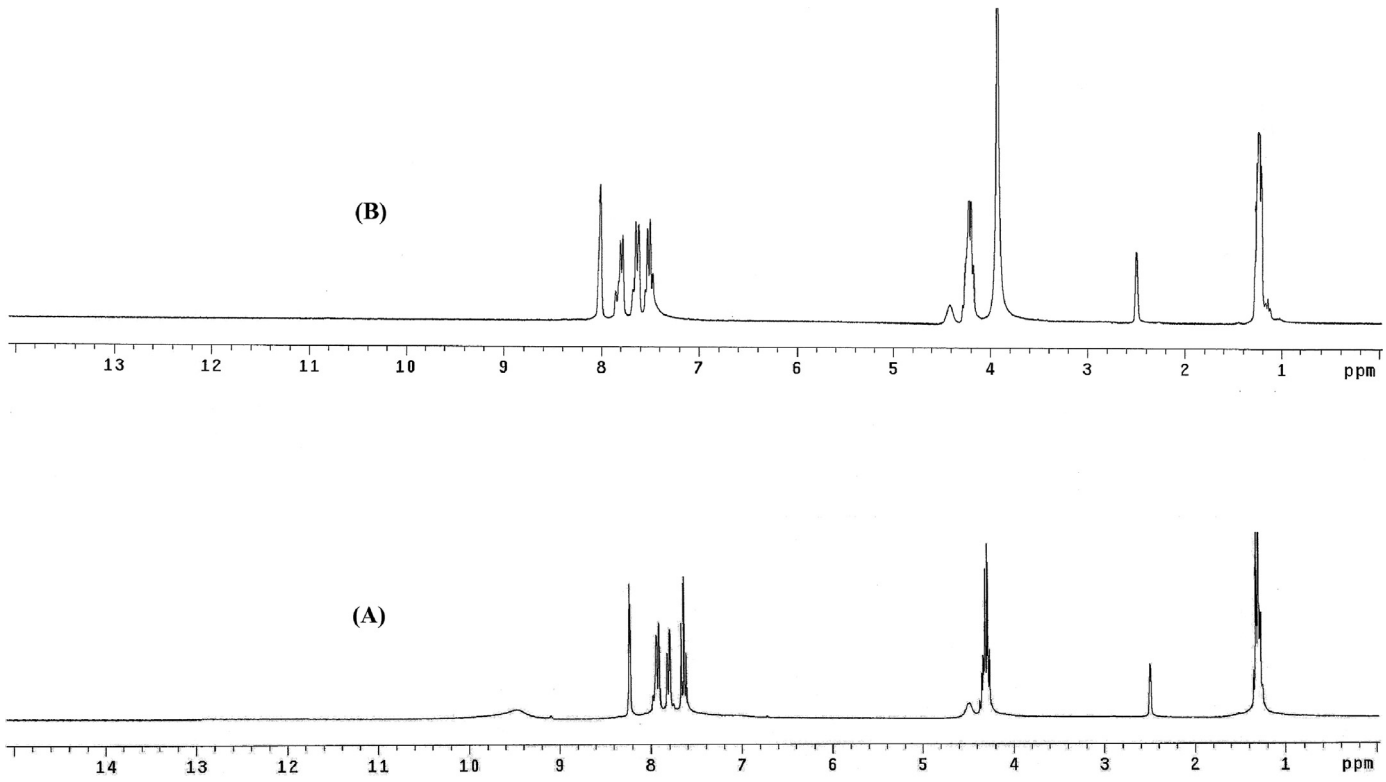

Fig. 4. ^{1}H NMR spectrum of 1: (A) in DMSO; (B) in DMSO + D_2O.

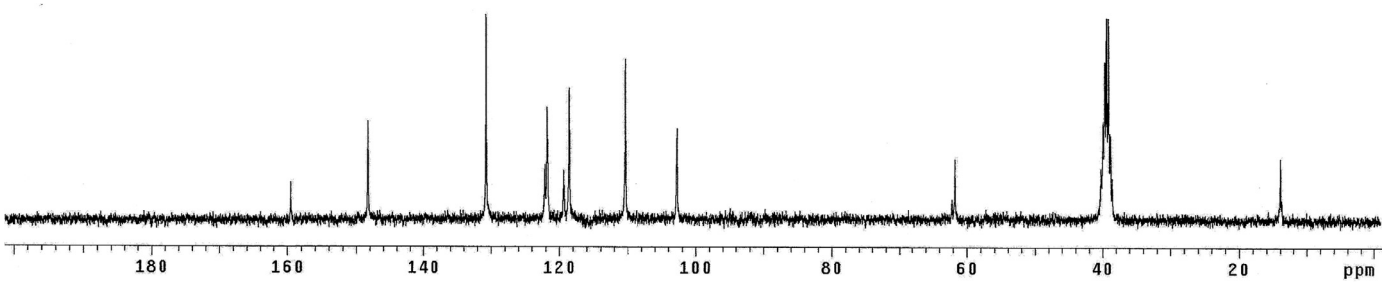

Fig. 5. ^{13}C NMR spectrum of 1.

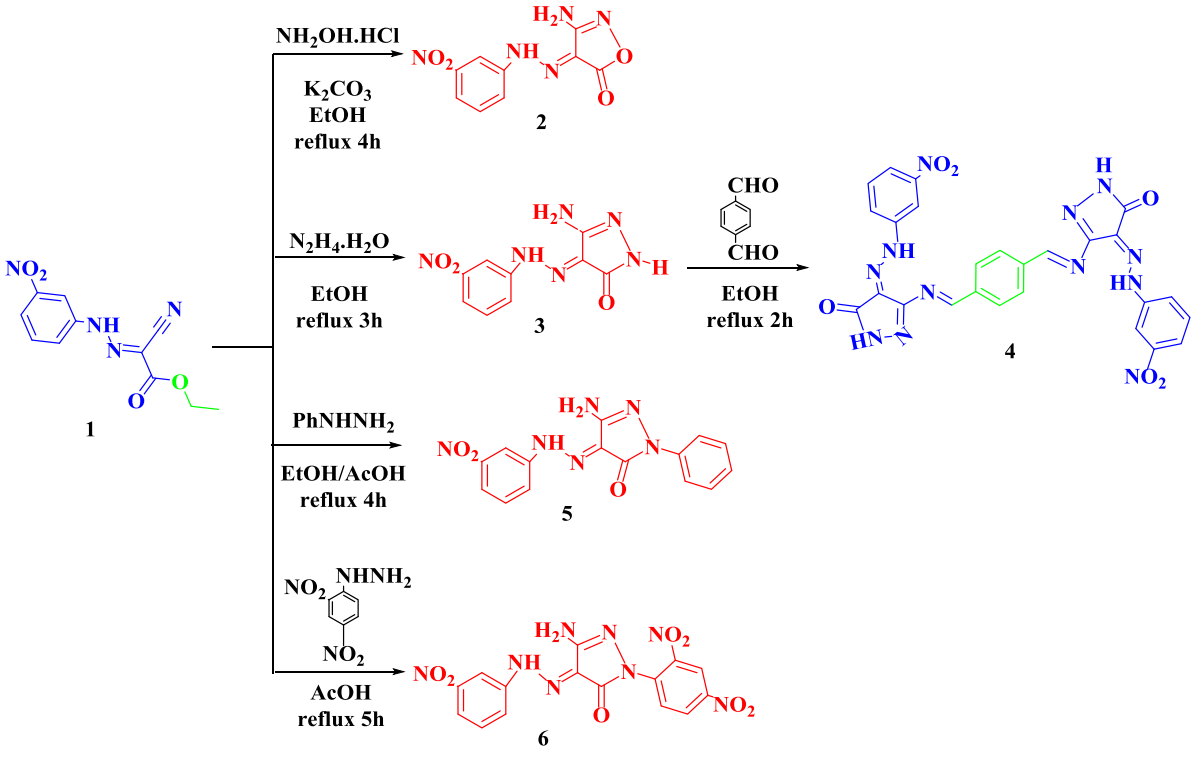

Scheme 2. Formation of isoxazolone, 2, and pyrazolone derivatives, 3–6.

The IR spectrum of compound **5** (**Fig. S17**) showed three broad medium bands at 3404, 3319 and 3167 cm^{-1} due to symmetric and asymmetric stretching frequencies of NH_2 and stretching frequency of NH, respectively. On the other hand, the mass spectrum of **5** displayed a molecular ion peak at *m/z* 325 [P^+] (61.18%). Also, the mass spectrum showed peaks at 309, 298, 278 and 252 corresponding to [P-NH_2]$^+$, [P-CO]$^+$, [P-NO_2]$^+$ and [P-H_2N–CN]$^+$ fragments. Interestingly, the ^{1}HNMR spectrum of **5** (**Figs. S18** and **S19**) showed very broad signal at 5.95 ppm along with two broad singlets at 12.35 and 12.89 ppm due to the NH_2 and NH protons. The line broadening of these signals indicated hydrogen exchange between the two groups through hydrogen bond formation. These signals disappeared on the addition of D_2O to the solution, which further confirming of the proton exchange. Compound **6** gave similar IR and ^{1}H NMR spectra (**Figs. S21–S23**) like compound **5**. This could be attributed to their structure similarities, Scheme 2. It is worth to mention that the signal of NH_2 group in the ^{1}HNMR spectrum of **6**, which was expected to appear around 6.0 ppm, collapsed in the base line with the appearance of two broad signals at 9.98 and 10.38 ppm due to hydrogen exchange between the NH_2 and NH protons. These two signals showed shift to higher field relative to those of **5**, probably due to the presence of two nitro groups in the phenyl ring attached to the pyrazolone ring.

As previously reported [46], we tried to synthesis the pyrimidine derivative **7** via the interaction of compound **1** with thiourea. However, the 1,2,4-triazine derivative **8** was found to be the isolated derivative (Scheme 3). Compound **8** probably formed through the speculated mechanism shown in Scheme 4. Structure of compound **8** was elucidated on the basis of its elemental analysis and spectral data. The IR spectrum of **8** (**Fig. S25**) exhibited bands at 3272, 2179, 1677 and 1605 cm^{-1} corresponding to the NH, C≡N, C = O and C = N functional groups, respectively. The mass spectrum of **8** also confirmed the molecular structure as it showed a peak at *m/z* = 276 (33.79%) due to the molecular ion parent peak. Although the IR spectrum of **8** showed a peak due to NH group, the ^{1}H NMR spectrum (**Fig. S26**) displayed no signal due to that group. This is probably due to the formation of hydrogen bonding with the adjacent carbonyl moiety [47]. Notably, reaction of compound **1** with phenyl isothiocyanate also gave the triazine derivative (5-oxo-3-thioxo-1,2,4-triazine-6-carbonitrile, **10**). Compound **10** may be formed through a nucleophilic attack of NH group of **1** on the isothiocyanate to give the intermediate **9**. Cy-

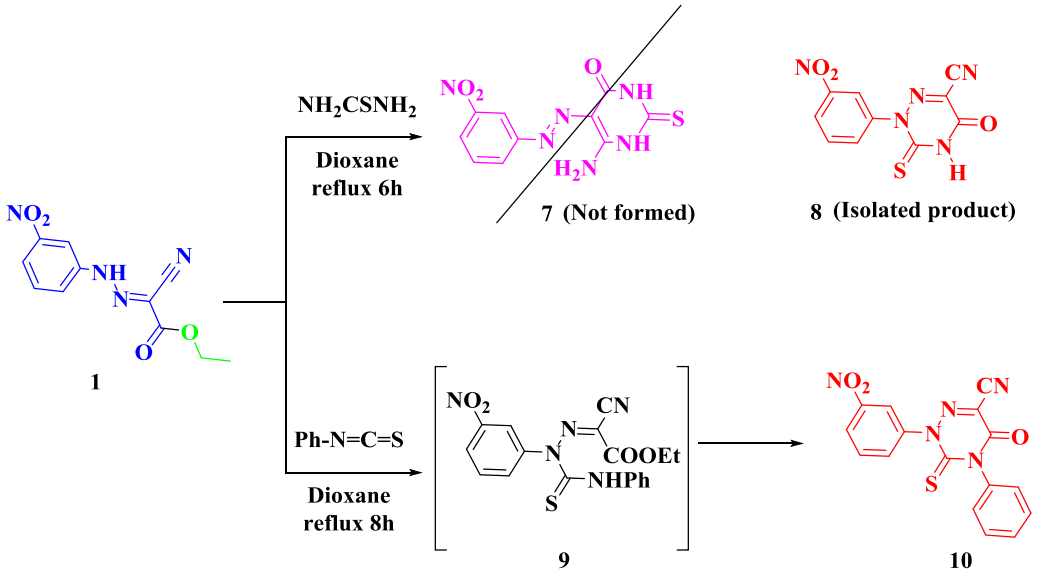

Scheme 3. Preparation of 1,2,4-triazine derivative, 8 and 10.

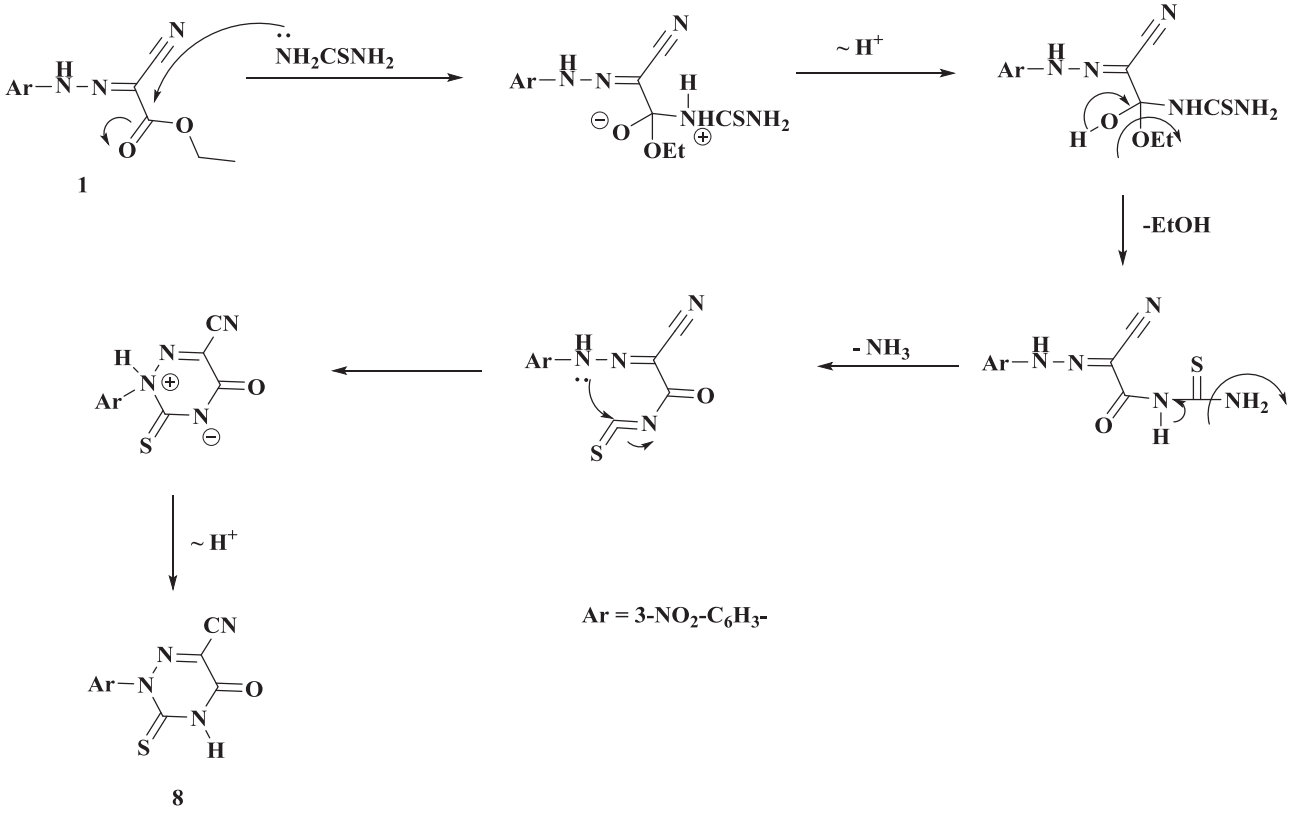

Scheme 4. Mechanism of formation of 1,2,4-triazine derivative, 8.

clization through elimination of one molecule of ethanol yielded compound **10** (Scheme 3).

Instead of the formation of the pyrazolone derivatives **11** and **12** [48], reactions of **1** with thiosemicarbazide and semicarbazide hydrochloride gave, interestingly, the unexpected 1,2,4-triazole derivatives **13** and **14**, respectively (Scheme 5). The two derivatives (**13** and **14**) presumably formed first via nucleophilic attack of the NH_2 group of carbazides on C = O of **1**, followed by removal of one molecule of ethanol. Further nucleophilic attack of the other NH_2 group of carbazide on the C = O of **1** with the removal of a water molecule would form the two derivatives. The IR spectra of the two derivatives (**Figs. S33** and **S37**) revealed existence of bands corresponding to C≡N groups and the absence of υ C = O of ester. In addition, the mass spectra showed molecular ion peaks at *m/z* 290 (7.79%) and 274 (56.24%) confirming the molecular formulas of the two compounds (**13** and **14**), respectively. The ^{1}H NMR spectra of **13** and **14** gave further emphasis to their structures. The ^{1}H NMR spectrum of **13** (**Figs. S34** and **S35**) displayed two broad signals at 8.58 and 4.48 ppm due to the two NH groups of the triazole ring. Interestingly, the latter signal exerted higher field shift and

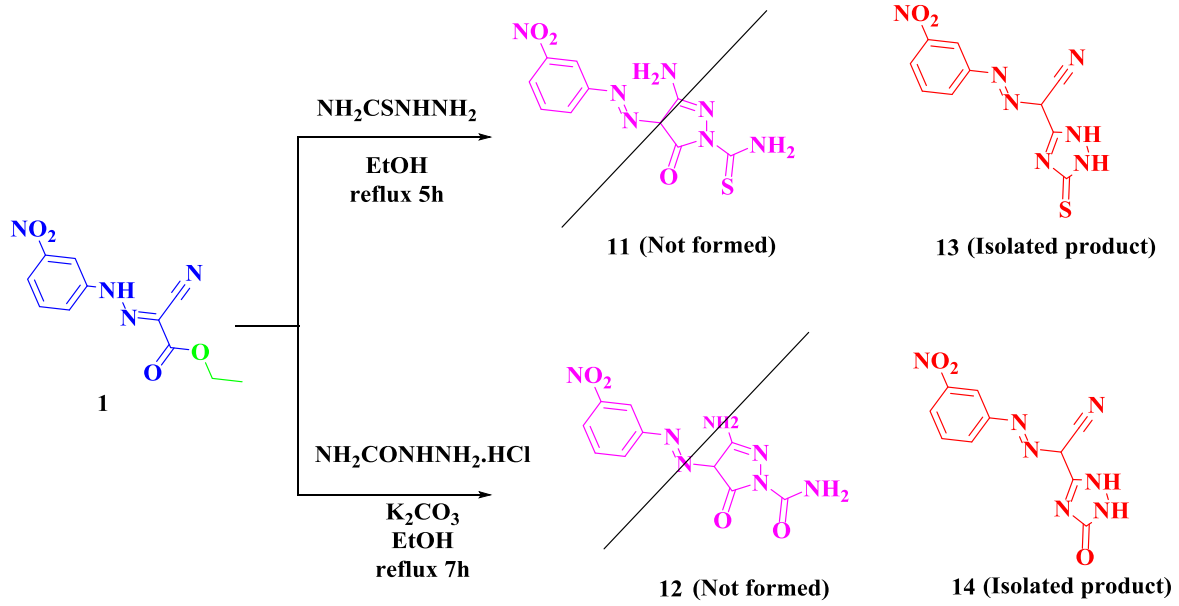

Scheme 5. Preparation of 1,2,4-triazole derivatives, 13 and 14.

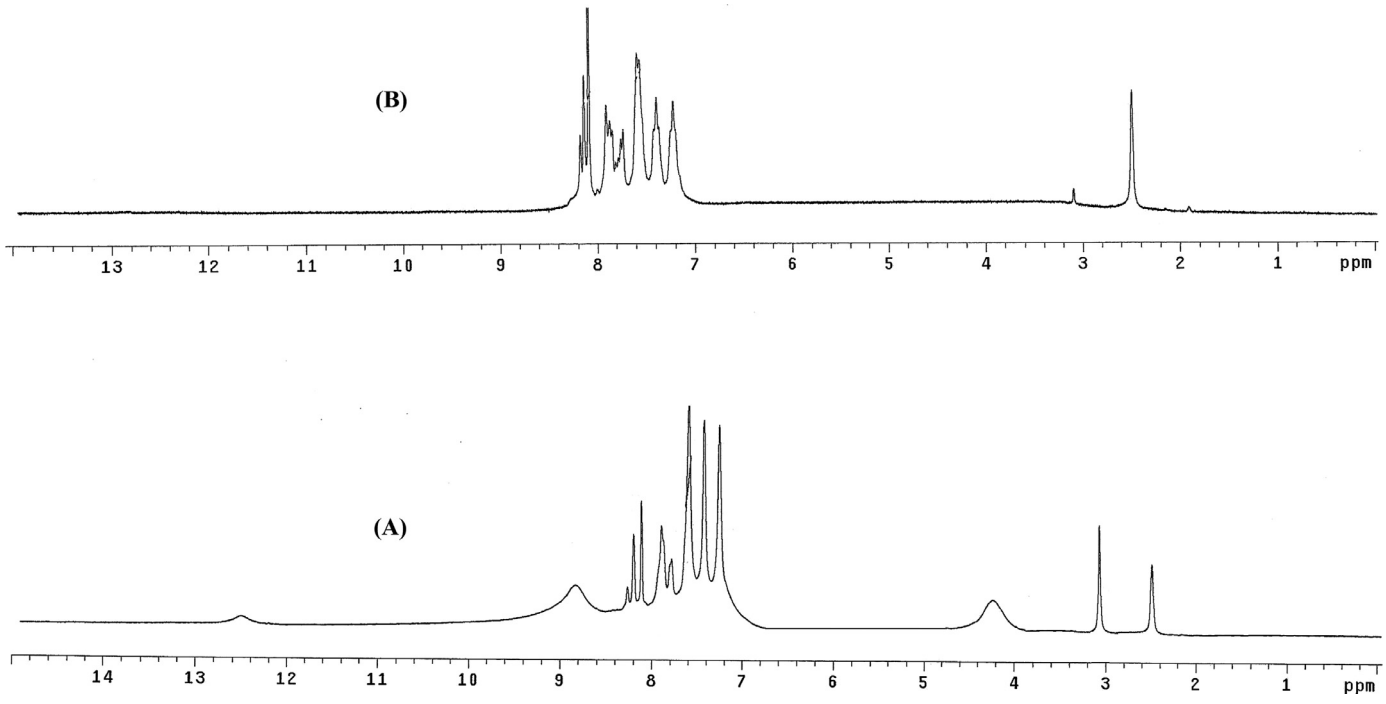

Fig. 6. ^{1}H NMR spectrum of 14: (A) in DMSO; (B) in DMSO + D_2O.

could be assigned to the NH group adjacent to the cyano moiety. On the other hand, the ^{1}H NMR spectrum of **14** (Fig. 6) showed, besides the two broad NH signals at 8.83 and 4.24 ppm, another broad signal at 12.45 ppm, which could be assigned as an OH signal. All the three signals disappeared on the addition of D_2O to the NMR solution (Fig. 6). The line broadening of the signals confirmed the fluxionality of the compound, *i.e.*, the three protons are exchangeable. Thus, it can be concluded that compound **14** existed in solution with two isomeric keto and enol forms in equilibrium (Scheme 5).

Interaction of compound **1** with 4-aminoazobenzene, 2-amino-3-hydroxypyridine, 2-aminothiazole, 3-amine-5-phenyl-1H-pyrazole, and 4-aminoantipyrine afforded the amide derivatives **15–19** (Scheme 7). The molecular formulas and structures of compounds were confirmed by using different analytical and spectroscopic techniques. The IR spectra exhibited the corresponding bands of the different functional groups (see experimental section) Scheme 6. However, the ^{1}H NMR spectra of compounds **16–19** showed dramatic changes. The ^{1}H NMR spectrum of **15** (**Figs. S42** and **S43**) showed two broad signals at 12.41 and 12.92 ppm, which they disappeared on the addition of deuterium oxide. These broad signals indicated the presence of keto/enol exchange in solution (Scheme 7). On the other hand, the ^{1}H NMR spectrum of **16** (**Figs. S46** and **S47**) showed only one broad signal (integration equivalent to four protons) with a range of 11.4–13.4 ppm and a signal average at 12.4 ppm. As indicated from Scheme 7,

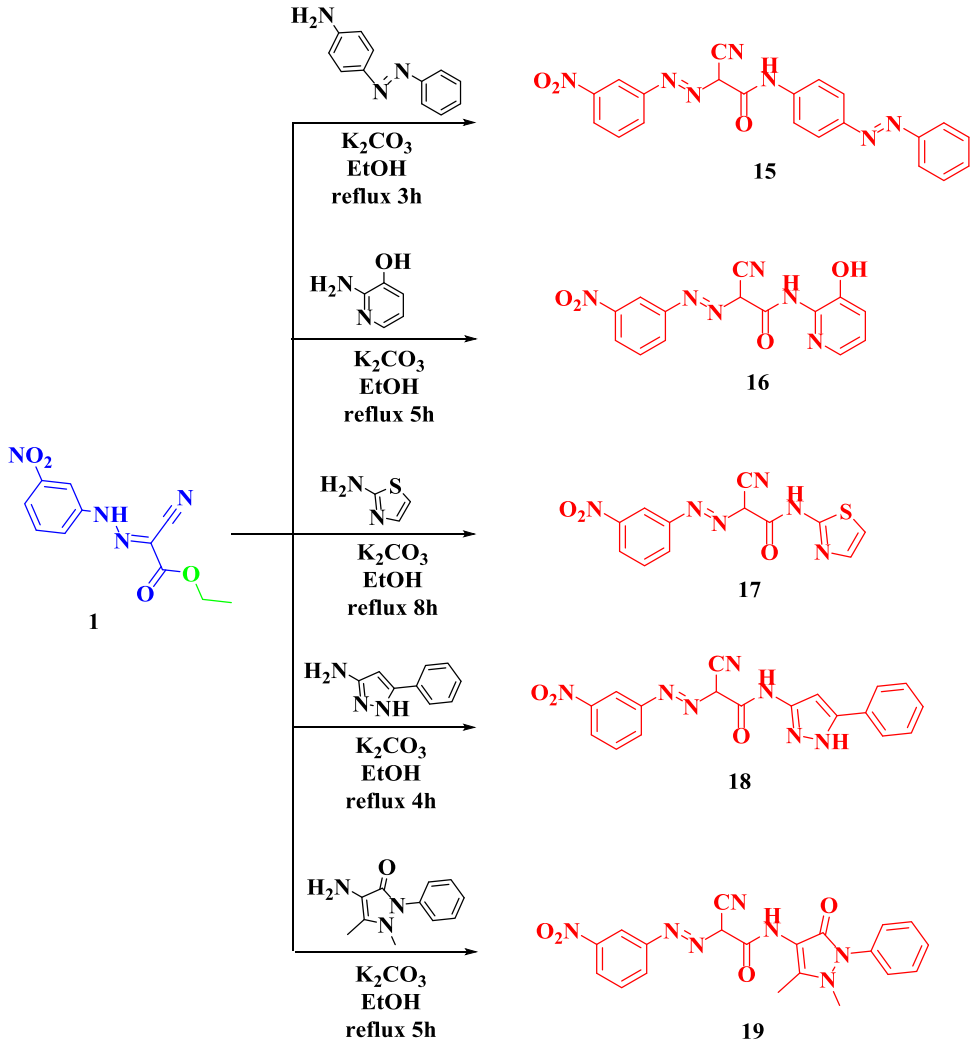

Scheme 7. Preparation of amide derivatives, 15–19.

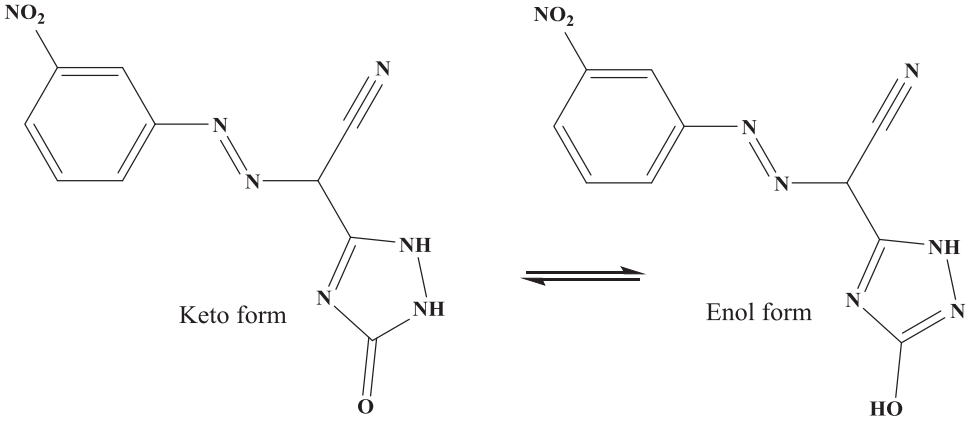

Scheme 6. Tautomeric keto/enol exchange in compound 14.

there is a fast exchange between the OH and NH protons of the two isomers in the NMR timescale. Because of this fast exchange, the expected four signals are averaged in one broad signal [49]. Similarly, the ^{1}H NMR spectrum of **17** (**Figs. S50** and **S51**) exhibited a broad signal (integration equivalent to two protons) with an average at 12.5 ppm and indicated fast exchange between the NH and OH protons of the keto and enol forms. In case of compound **18**, the ^{1}H NMR spectrum showed two signals at 5.81 and 11.29 ppm. These two signals could be assigned for the NH proton of the pyrazole ring and OH proton, respectively. Therefore, it can be concluded that compound **18** existed in solution as an enol form (Scheme 7). Interestingly, the IR spectrum for **18** (**Fig. S53**) gave bands at 3299, 3024 and 1692 cm^{-1} for NH and C = O, which confirmed the presence of keto form in solid state. Compound **19**, also, behaved similarly like compound **18**. Its ^{1}H NMR spectrum showed only a signal at 12.34 ppm for OH proton in an enol form.

Table 3
Comparison between the physical data of the synthesized compounds under thermal, grinding and microwave reaction conditions.

Compound*	Time (min)			% Yield			YE			RME			OE			AE
	Th.	G.	M.W.	Th.	G.	M.W.	Th.	G.	M.W.	Th.	G.	M.W.	Th.	G.	M.W.	
1	60	–	–	57	–	–	0.95	–	–	62.46	–	–	84.75	–	–	73.70
2	240	8	1	61	84	93	0.2542	10.50	93.00	30.94	40.61	44.97	58.28	76.49	84.71	53.09
3	180	9	2	62	80	94	0.3444	8.89	47.00	42.95	55.41	65.12	54.04	69.72	81.93	79.48
4	120	10	2	59	77	91	0.4917	7.70	45.50	51.84	67.66	79.96	54.98	71.76	84.80	94.29
5	240	8	3	57	79	95	0.2375	9.88	31.67	38.80	53.77	64.66	44.26	61.33	73.75	87.67
6	300	9	4	60	83	90	0.2000	9.22	22.50	47.77	66.08	71.65	53.08	73.42	79.61	90.00
8	360	–	–	61	–	–	0.1694	–	–	39.75	–	–	48.86	–	–	81.36
10	480	7	1	59	81	94	0.1229	11.57	94.00	43.05	59.11	68.59	48.69	66.86	77.58	88.41
13	300	–	–	62	–	–	0.2067	–	–	44.91	–	–	54.86	–	–	81.87
14	300	–	–	64	–	–	0.2133	–	–	31.37	–	–	58.72	–	–	53.42
15	180	9	3	66	79	92	0.3667	8.78	30.67	42.39	50.74	59.09	61.27	73.34	85.41	69.18
16	300	10	4	59	80	93	0.1967	8.00	23.25	34.59	46.91	54.53	54.11	73.39	85.31	63.92
17	480	13	4	61	83	95	0.1271	27.67	23.75	35.30	48.04	54.98	55.85	76.01	86.99	63.20
18	240	8	2	62	86	91	0.2583	10.75	45.50	38.43	53.31	56.40	57.29	79.47	84.08	67.08
19	300	9	2	60	87	93	0.2000	9.67	46.50	38.74	56.17	60.04	55.75	80.83	86.40	69.49

* Th., thermal; G, grinding; M.W., microwave irradiation; YE, yield economy; RME, reaction mass efficiency; OE, optimum efficiency; AE, atom economy.

The IR spectrum indicated the existence of keto form in the solid state.

3.3. Comparison between convention, microwave and grinding reactions

The green chemistry approach is the science of design of chemical processes that reduce or eliminate the generation of hazardous compounds. Thus, it prevents pollution at the molecular level. The use of microwave irradiation and grinding techniques in syntheses of chemical compounds are also branches of the green chemistry processes. Notably, microwave-assisted synthesis received much interest in many recent researches because the chemical transformations within it are usually pollution-free, eco-friendly and offer high yields together with simplicity in processing and handling [50,51]. In contradictory, thermal reactions with conventional technique are slow and may be responsible for the possible decomposition of products, substrates and reagents. Herein, the reported derivatives were synthesized via three different (thermal, grinding and microwave) techniques (Table 3). In the following section, comparison between some physical data of those synthesized compounds isolated from grinding and microwave reactions with the conventional thermal reactions are given. (The reaction completion in the all three techniques was indicated by applying TLC method). Comparison were in terms of yield economy (YE), atom economy (AE), reaction mass efficiency (RME) and optimum efficiency (OE) to express the efficiency of the reactants to give the desired product. Yield economy is a metric to assess the conversion efficiency of the different synthetic techniques of the same reaction. YE measures how much yield of a desired product is obtained over a certain reaction time and is calculated from the equation: YE = [% Yield / Reaction time (min)]. A higher YE is indicative of a higher level of conversion, more efficient chemical process, and more economical reaction. RME is measured by the mass of the isolated product divided by the mass of reactants. AE gives the theoretical maximum efficiency of reactant utilization. OE is used for the direct comparisons of two reaction types and is derived from the relation between RME and AE (RME/AE × 100). Details of the calculations of these parameters are previously reported [52,53]. As can be seen from Table 3, the percentage yield obtained from microwave and grinding reactions are higher than that obtained from the conventional thermal reactions. Notably, the% yield obtained from the microwave-assisted synthesis approached stoichiometric completion. In addition, the microwave and grinding reactions afforded better reaction mass efficiency and optimum efficiency than those of thermal reactions.

3.4. Biological activity studies

3.4.1. Antibacterial activity

The *in vitro* antibacterial activities of some selected derivatives (**2, 3, 8, 13** and **17**) were screened against two bacteria (*E. coli* and *Bacillus subtilis*), and compared with Ampicillin as an antibacterial drug. The inhibition zone (mm) and percentage activity index of the tested compounds are tabulated in Table 4. The percentage activity index was calculated using the following formula:

$$\%\ Activity\ index = \frac{Zone\ of\ inhibition\ by\ tested\ compound}{Zone\ of inhibition\ by\ s\tan dard}$$

The results indicated moderate antibacterial activities for the tested derivatives with respect to the standard. Such activities can be explained by the cell permeability concept [54]. The data showed that the screened compounds have the capacity of inhibiting the metabolic growth of the investigated bacteria to different extents, which may indicate broad-spectrum properties. The activity of these compounds may arise from the presence of NH, CN and C = O groups. The mode of action may involve formation of hydrogen bonding between those functional groups and the active centers of the cell constituents, leading to interference with the normal cell process [55–57]. As the cell membrane has been made from lipid layers that are permeable only for lipid-soluble materials. Therfore, the lipophilicity character plays an important factor that affect the bacteria inhibition. As a result, the decreased lipophilicity would thus depress the inhibition ability of the tested compound.

3.4.2. In vitro *cytotoxicity studies*

Cell viability study is the primary procedure to understand the cytotoxicity profile of any new chemical entity [58]. The chemotherapeutic potential of some of the reported compounds (**2, 3, 8, 13** and **17**) as promising anticancer agents was evaluated by measuring their abilities to inhibit two human cell lines (liver carcinoma cell line, HePG-2, and breast cancer cell line, MCF-7) using Doxorubicin as a reference drug control. Doxorubicin is a chemotherapy drug called an anthracycline. It slows or stops the growth of cancer cells by blocking an enzyme called topo isomerase 2. The IC_{50} (concentration that produce 50% inhibition of cell growth) values of the tested compounds qualitatively determine the strength of anticancer drug. It is well known that compounds that exhibit IC_{50} values more than 30 μM are considered weak anticancer drugs while, those show IC_{50} values lower than 25 μM are believed to be moderate to strong antitumor agents [59]. The IC_{50} values of the studied derivatives along with those

Table 4
In vitro antibacterial activities of the studied compounds.

Compound	E. coli		Bacillus subtilis	
	Inhibition zone (mm)	% Activity index	Inhibition zone (mm)	% Activity index
2	7	26.9	8	34.8
3	10	38.5	12	52.2
8	4	15.4	5	21.7
13	14	53.8	11	47.8
17	–	–	3	13.0
Ampicillin	26	100	23	100

Table 5
The IC_{50} values of the reported compounds and the Doxorubicin standard.

Compound	*In vitro* cytotoxicity IC_{50} (μM)	
	HePG-2	MCF7
2	45.93 ± 3.1	41.48 ± 2.9
3	26.17 ± 2.2	32.29 ± 2.4
8	63.08 ± 3.6	52.16 ± 3.3
13	38.20 ± 2.7	19.35 ± 1.6
17	74.56 ± 3.9	65.32 ± 3.5
Doxorubicin	4.50 ± 0.2	4.17 ± 0.2

of the standard were determined and given in Table 5. The compounds showed moderate to weak activities against the studied cell lines. Notably, the two compounds **3** and **13** exhibited better IC_{50} values relative to the other derivatives. The results revealed that the investigated compounds attenuated the two types of cancer cells proliferation in different selectivity, and the inhibition effects were enhanced in a concentration dependent fashion. These observations reflect the effect of the studied compounds on changing the morphology of the cancer cell lines, and this behavior may be associated to the higher DNA binding affinity and could presumably occur through the formation of charge transfer complexes or hydrogen bonding. Although the IC_{50} values of the reported compounds are smaller than those of standard, further *in vivo* studies are required to evaluate the potency of these derivatives as antitumor reagents.

3.5. Molecular docking studies

Molecular docking is a considerable approach to understand the interaction between molecularly designed small compounds and biological targets. Analysis of the docking data is useful in predicting the conformational changes associated with residues, such as amino acids, at the binding position to accommodate the docked hydrophobic inhibitors. Some selected compounds (**2, 3, 8, 13** and **17**) were subjected to molecular docking studies using the MOE version 2014.0901 to understand the compound-DNA interactions and to explore the potential binding mode and energy. The docked

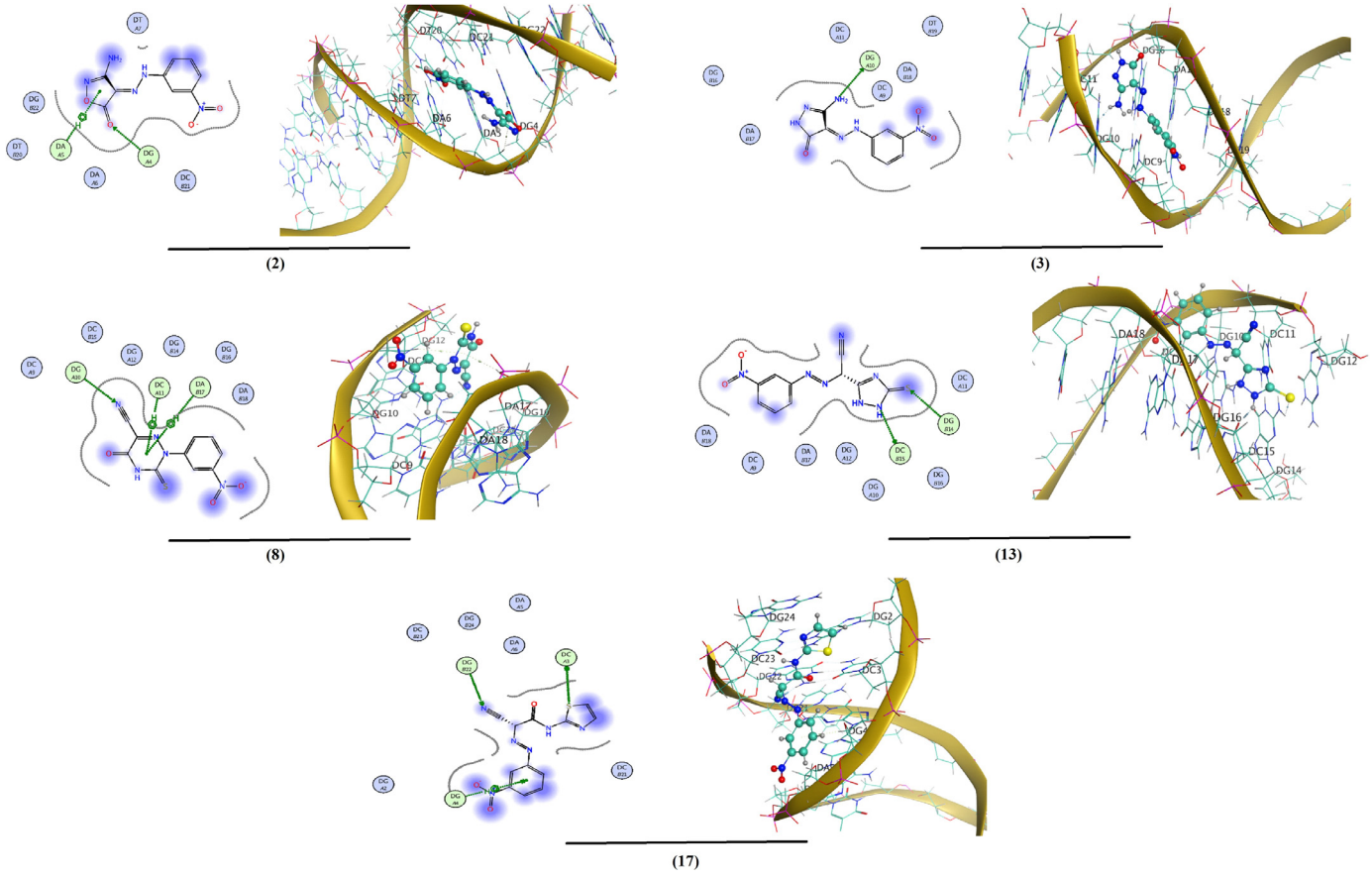

Fig. 7. The 2D and the 3D representations of the interaction of investigated compounds with DNA.

Table 6
The molecular docking data of the reported compounds.

Compound	S (kcal/mol)	rmsd value [a]	Ligand-Receptor	Interaction type	Interaction distance, Å	E (kcal/mol)
2	- 4.712	1.33	O15-N2 (DG 4)	H-acceptor	3.03	−3.3
			5-ring-C4′ (DA 5)	π-H	4.48	−0.7
3	−6.398	0.85	N14-N3 (DG 10)	H-donor	3.41	−0.8
8	−4.162	1.51	N20-N2 (DG 10)	H-acceptor	3.43	−0.7
			6-ring-C4′ (DC 11)	π-H	3.96	−1.0
			6-ring-C4′ (DA 17)	π-H	3.90	−1.3
13	−5.846	1.36	N14-O2 (DC 15)	H-donor	3.03	−4.8
			S15-N2 (DG 14)	H-acceptor	3.51	−1.0
17	−5.683	1.28	S17-O4′ (DC 3)	H-donor	4.24	−0.5
			N22-N2 (DG 22)	H-acceptor	3.31	−3.0
			6-ring-C4′ (DG 4)	π-H	4.43	−0.6
			O19-N2 (DG 4)	H-acceptor	3.38	−0.8

ligands conformations were rated according to the binding energy score, hydrogen bonding and hydrophobic interactions between the compounds and a B-DNA (PDB ID:1BNA). The docking studies determine the way by which the docked compounds fundamentally fit in the DNA minor groove and comprise of hydrophobic, ionic, and hydrogen bonding interactions with the DNA bases (Fig. 7). The binding poses can be evaluated by a scoring function (S), which determines the obtained poses. (Scoring functions are mathematical functions used to approximately predict the binding affinity between two molecules after they are docked). The score values are usually negative, and the more negative value implies that docked ligand has higher binding affinity to the target. The investigated compounds showed good binding scores, with high negative values. These negative values reflect high binding affinity between the DNA target and molecules indicating good efficiency of the compounds as bioactive materials. The molecular docking data including the score and rmsd values (the root mean square deviation, which is the measure of the average distance between the docked atoms), interaction type and energy are given in Table 6. It was found that the most of the optimal docking results were in the DG, DC and DA regions of the DNA. The binding interactions came from either hydrophobic interactions between the amino acid residues such as DA, DC and DG with the aromatic moieties of the ligands or from the hydrogen bonds (H-donor, H-acceptor and π-H) formed between the DNA residues and molecules (Fig. 7 and Table 6). The order of increasing of binding interaction is as follows: **8** < **2** < **17** < **13** < **3**. Interestingly, this order is correlated with the antibacterial and cytotoxicity data of the compounds (*vide supra*).

4. Conclusion

Conventional thermal synthesis as well as microwave and grinding green synthesis of some molecularly designed isoxazolone, pyrazolone, triazine, triazole and amide derivatives were carried out. Comparison between the three reaction routs confirmed the advantage of the one-pot synthesis over the traditional thermal technique. Spectroscopic studies showed different structural features for these derivatives. ^{1}H NMR data revealed that compounds, such as **2, 5, 8, 14** and **17**, displayed hydrogen bonding between the NH and NH_2 protons, and they were found to be exchangeable. Molecular geometry optimization and the calculated quantum global descriptors of some compounds identified their interesting geometrical configurations and reactivity. The existence of H-bonding between the NH or NH_2 moieties in the optimized structures confirmed the spectroscopic findings. Antibacterial (*E. coli* and *Bacillus subtilis*) and cytotoxicity screening of two human cell lines (HePG-2 and MCF-7) for some selected compounds suggested their potency as potential antibacterial and antitumor reagents. Molecular docking of some compounds illustrated their possible performance as bioactive materials and their DNA binding potency. The tested compounds illustrated high negative binding scoring (−4.162 to −6.398), which reflect the high binding affinities towards the DNA receptor.

Declaration of Competing Interest

The authors declare that they have no known competing financial interests or personal relationships that could have appeared to influence the work reported in this paper.

Supporting information

Additional supporting information may be found online in the Supporting Information section at the end of this article.

Supplementary materials

Supplementary material associated with this article can be found, in the online version, at doi:10.1016/j.molstruc.2022.132513.

CRediT authorship contribution statement

Kurls E. Anwer: Investigation, Methodology, Writing – original draft. **Galal H. Sayed:** Data curation, Supervision, Writing – original draft. **Ramadan M. Ramadan:** Conceptualization, Supervision, Validation, Writing – review & editing.

References

[1] S. Benkhaya, S. M'rabet, A. El Harfi, Classifications, properties, recent synthesis and applications of azo dyes, Heliyon 6 (2020) e03271, doi:10.1016/j.heliyon.2020.e03271.
[2] K. Bhuvaneswari, N. Nagasundaram, A. Lalitha, Synthesis, anti-inflammatory activity, and molecular docking study of novel azo bis antipyrine derivatives against cyclooxygenase-2 enzyme, J. Chin. Chem. Soc. 68 (2021) 27–33.
[3] L.R. Jeppson, H.H. Keifer, E.W. Baker, Acaricides used for control of agricultural mites, Mites Injurious to Economic Plants, University of California Press, 2020.
[4] Z.A. Bhavsar, P.T. Acharya, D.J. Jethava, H.D. Patel, Recent advances in development of anthelmintic agents: synthesis and biological screening, Synth. Commun. 50 (2020) 917–946.
[5] G. Maleeva, A. Nin-Hill, K. Rustler, E. Petukhova, D. Ponomareva, E. Mukhametova, A.M.J. Gomila, D. Wutz, M. Alfonso-Prieto, B. König, P. Gorostiza, P. Bregestovski, Subunit-specific photocontrol of glycine receptors by azobenzene-nitrazepam photoswitcher, eNeuro 8 (2021), doi:10.1523/ENEURO.0294-20.2020.
[6] T.T.M. Ashfaq, M.I. Shahzad, R. Tabassum, Antiviral evaluation of bioactive azo derivatives to treat endemic poultry viruses, Thai J. Vet. Med. 50 (2020) 435–443.
[7] Y. Nuruki, H. Matsumoto, M. Tsukada, H. Tsukahara, T. Takajo, K. Tsuchida, K. Anzai, Method to improve azo-compound (AAPH)-induced hemolysis of erythrocytes for assessing antioxidant activity of lipophilic compounds, Chem. Pharmaceut. Bull. 69 (2021) 67–71.
[8] H.A. Naseem, T. Aziz, K. Ahmad, S. Parveen, M. Ashfaq, Rational synthesis and characterization of medicinal phenyl diazenyl-3-hydroxy-1h-inden-1-one azo derivatives and their metal complexes, J. Mol. Struct. 1227 (2021) 129574.
[9] J.D. Tadić, J.M. Lađarević, Ž.J. Vitnik, V.D. Vitnik, T.P. Stanojković, I.Z. Matić, D.Ž. Mijin, Novel azo pyridone dyes based on dihydropyrimidinone skeleton: synthesis, DFT study and anticancer activity, Dyes Pigments 187 (2021) 109123.

[10] A. Sailer, F. Ermer, Y. Kraus, R. Bingham, F.H. Lutter, J. Ahlfeld, O. Thorn-Seshold, Potent hemithioindigo-based antimitotics photocontrol the microtubule cytoskeleton in cellulo, Beilstein J. Org. Chem. 16 (2020) 125–134.

[11] M.J. Burgess, R.A. Sewell, D.P. Clifford. U.S. Patent No. 4, 800, 195 (1989). Washington, DC: U.S. Patent and Trademark Office

[12] G.H. Sayed, N.A. Negm, M.E. Azab, K.E. Anwer, Synthesis, characterization and biological activity of some pyrazole-pyrazolone derivatives, Egypt. J. Chem. 59 (2016) 663–672.

[13] W.A. Fadaly, Y.A. Elshaier, E.H. Hassanein, K.R. Abdellatif, New 1, 2, 4-triazole/pyrazole hybrids linked to oxime moiety as nitric oxide donor celecoxib analogs: synthesis, cyclooxygenase inhibition anti-inflammatory, ulcerogenicity, anti-proliferative activities, apoptosis, molecular modeling and nitric oxide release studies, Bioorg. Chem. 98 (2020) 103752.

[14] D. Huang, M. Huang, A. Liu, X. Liu, W. Liu, X. Chen, H. Xue, J. Sun, D. Yin, X. Wang, Design, synthesis, and acaricidal activities of novel pyrazole acrylonitrile compounds, J. Heterocycl. Chem. 54 (2017) 1121–1128.

[15] R. Kenchappa, Y.D. Bodke, Synthesis, analgesic and anti-inflammatory activity of benzofuran pyrazole heterocycles, Chem. Data Collect. 28 (2020) 100453.

[16] Y. Jiao, S. Preston, H. Song, A. Jabbar, Y. Liu, J. Baell, A. Hofmann, D. Hutchinson, T. Wang, A.V. Koehler, G.M. Fisher, K.T. Andrews, B. Laleu, M.J. Palmer, J.N. Burrows, T.N.C. Wells, Q. Wang, R.B. Gasser, Assessing the anthelmintic activity of pyrazole-5-carboxamide derivatives against Haemonchus contortus, Parasites Vectors 10 (2017) 272, doi:10.1186/s13071-017-2191-8.

[17] C.A. Dvorak, J. Liang, N.S. Mani, N.I. Carruthers, Regioselective assembly of fused pyrazole-azepine heterocycles: synthesis of the 5-HT7 antagonist 1-benzyl-3-(4-chlorophenyl)-1,4,5,6,7,8-hexahydropyrazolo [3, 4-d] azepine, Tetrahedron Lett. (2021) 152843.

[18] G. Yang, H. Zheng, W. Shao, L. Liu, Z. Wu, Study of the *in vivo* antiviral activity against TMV treated with novel 1-(t-butyl)-5-amino-4-pyrazole derivatives containing a 1,3,4-oxadiazole sulfide moiety, Pesticide Biochem. Physiol. 171 (2021) 104740.

[19] S. Naveen, K. Kumara, A.D. Kumar, K.A. Kumar, A. Zarrouk, I. Warad, N.K. Lokanath, Synthesis, characterization, crystal structure, Hirshfeld surface analysis, antioxidant properties and DFT calculations of a novel pyrazole derivative: ethyl 1-(2,4-dimethylphenyl)-3-methyl-5-phenyl-1H-pyrazole-4-carboxylate, J. Mol. Struct. 1226 (2021) 129350.

[20] Q. Fu, S.J. Kang, L.K. Zhong, J. Chen, C.X. Tan, J.Q. Weng, T.M. Xu, X.H. Liu, Synthesis and herbicidal activity of new pyrazole ketone derivatives, Phosphorus Sulfur Silicon Relat. Elem. 196 (2021) 200–205.

[21] S. Mohamed, N. Dawoud, S.N. Shabaan, N. Fathall, G. Hosni, K.E. Anwer, Synthesis and biological activity of a new class of enaminonitrile pyrazole, Egypt. J. Chem. 64 (2021) 9–10.

[22] V. Kumar, Y.N. Spoorthy, L.K. Rvindranath, Molecular docking, synthesis, characterisation and *in vitro* anti-mitotic evaluation of some novel pyrrole and pyrazole derivatives of purine, IJAR 6 (2020) 136–156.

[23] K.N. Halim, S.K. Ramadan, S.A. Rizk, M.A. El-Hashash, Synthesis, DFT study, molecular docking and insecticidal evaluation of some pyrazole-based tetrahydropyrimidine derivatives, Synth. Commun. 50 (2020) 1159–1175.

[24] G.H. Sayed, M.E. Azab, K.E. Anwer, M.A. Raouf, N.A. Negm, Pyrazole, pyrazolone and enaminonitrile pyrazole derivatives: synthesis, characterization and potential in corrosion inhibition and antimicrobial applications, J. Mol. Liq. 252 (2018) 329–338.

[25] K. Kumara, M.G. Prabhudeva, C.B. Vagish, H.K. Vivek, K.M.L. Rai, N.K. Lokanath, K.A. Kumar, Design, synthesis, characterization, and antioxidant activity studies of novel thienyl-pyrazoles, Heliyon 7 (2021) e07592.

[26] C.B. Vagish, K. Kumara, H.K. Vivek, S. Bharath, N.K. Lokanath, K.A. Kumar, Coumarin-triazole hybrids: design, microwave-assisted synthesis, crystal and molecular structure, theoretical and computational studies and screening for their anticancer potentials against PC-3 and DU-145, J. Mol. Struct. 1230 (2021) 129899.

[27] V. Channabasappa, K. Kumara, A.K. Kariyappa, Design, synthesis of coumarin tethered 1, 2, 3-triazoles analogues, evaluation of their antimicrobial and α-amylase inhibition activities, J. Chem. Sci. 133 (2021) 1–8.

[28] J. Muškinja, N. Janković, R. Zoran, G.A. Bogdanović, Z.M. Bugarčić, Vanillic aldehydes for the one-pot synthesis of novel 2-oxo-1,2,3,4-tetrahydropyrimidines, Mol. Divers 20 (2016) 591–604.

[29] G.H. Sayed, M.E. Azab, K.E. Anwer, Conventional and Microwave-assisted synthesis and biological activity study of novel heterocycles containing pyran moiety, J. Heterocycl. Chem. 56 (2019) 2121–2133.

[30] K. Anwer, G. Sayed, H. Hassanan, M. Azab, Conventional and microwave synthesis of some new pyridine derivatives and evaluation of Their antimicrobial and cytotoxic activities, Egypt. J. Chem. 62 (2019) 707–726.

[31] K.E. Anwer, G.H. Sayed, Conventional and microwave reactions of 1, 3-diaryl-5, 4-enaminonitrile-pyrazole derivative with expected antimicrobial and anticancer activities, J. Heterocycl. Chem. 57 (2020) 2339–2353.

[32] M.J. Frisch, H.B. Schlegel, G.E. Scuseria, M.A. Robb, J.R. Cheeseman, G.Scalmani, V.Barone, B. Mennucci, G.A. Petersson, H. Nakatsuji, M. Caricato, X.Li, H.P.Hratchian, A.F. Izmaylov, J. Bloino, G. Zheng, J.L. Sonnenberg, M. Hada, M. Ehara, K. Toyota, R. Fukuda, J. Hasegawa, M. Ishida, T. Nakajima, Y. Honda, O. Kitao, H. Nakai, T. Vreven, J.A. Montgomery, J.E. Peralta, F. Ogliaro, M. Bearpark, J.J. Heyd, E. Brothers, K.N. Kudin, V.N. Staroverov, R. Kobayashi, J. rmand, K. Raghavachari, A. Rendell, J.C. Burant, S.S. Iyengar, J. Tomasi, M. Cossi, N. Rega, J.M. Millam, M. Klene, J.E. Knox, J.B. Cross, V. Bakken, C. Adamo, J. Jaramillo, R. Gomperts, R.E. Stratmann, O. Yazyev, A.J. Austin, R. Cammi, C. Pomelli, J.W. Ochterski, R.L. Martin, K. Morokuma, V.G. Zakrzewski, G.A. Voth, P. Salvador, J.J. Dannenberg, S. Dapprich, A.D. Daniels, O. Farkas, J.B. Foresman, J.V. Ortiz, J. Cioslowski and D.J. Fox, Gaussian Inc., Wallingford, CT (2009).

[33] R.G. Mohamed, A.A. Makhlouf, S.A. Mosad, A.A. Abdel Aziz, S.M. El-Medani, R.M. Ramadan, Spectroscopic, DFT, biological, DNA binding and antioxidant studies of some metal chelates with a novel thiazole derived Schiff base, J. Coord. Chem. 71 (2018) 3665–3688.

[34] C.M. Lozano, O. Cox, M.M. Muir, J.D. Morales, J.L. Rodriguez-Cabain, P.E. Vivas-Mejfa, F.A. Gonzalez, Cytotoxic anionic tribromo platinum(II) complexes containing benzothiazole and benzoxazole donors: synthesis, characterization, and structure-activity correlation, Inorg. Chim. Acta 271 (1998) 137–144.

[35] R.M. Ramadan, K. Abu Al-Nasr, A.F.H. Noureldeen, Synthesis, spectroscopic studies, antimicrobial activities and antitumor of a new monodentate V-shaped Schiff base and its transition metal complexes, Spectrochim. Acta Part A 132 (2014) 417–422.

[36] K.L. Jyothi, K. Kumara, M.K. Hema, R. Gautam, T.G. Row, N.K. Lokanath, Structural elucidation, theoretical insights and thermal properties of three novel multicomponent molecular forms of gallic acid with hydroxypyridines, J. Mol. Struct. 1207 (2020) 127828.

[37] R.M. Ramadan, S.M. El-Medani, A.A. Makhlouf, H. Moustafa, M.A. Afifi, M. Haukka, A.A. Abdel Aziz, Spectroscopic, DFT, non-linear optical properties and *in vitro* biological studies of Co(II), Ni(II) and Cu(II) complexes of hydrazide Schiff base derivatives, Appl. Organometal. Chem. (2021) e6246.

[38] C. Shruthi, V. Ravindrachary, B. Guruswamy, D.J. Prasad, J. Goveas, K. Kumara, N.K. Lokanath, Molecular structure, Hirshfeld surface and density functional theoretical analysis of a NLO active chalcone derivative single crystal – A quantum chemical approach, J. Mol. Struct. 1228 (2021) 129739.

[39] S. Hassen, H. Chebbi, M.F. Zid, Y. Arfaoui, Assembly and weak interactions in the crystal structure of 2-amino-4-(3-bromophenyl)-1,3,5-triazinobenzimidazolium chloride studied by X-ray diffraction, vibrational spectroscopy, Hirshfeld surface analysis and DFT calculations, J. Mol. Struct. 1179 (2019) 678–684.

[40] M. Yıldız, Ö. Karpuz, C.T. Zeyrek, B. Boyacıoğlu, H. Dal, N. Demir, N. Yıldırım, H. Ünver, Synthesis, biological activity, DNA binding and anion sensors, molecular structure and quantum chemical studies of a novel bidentate Schiff base derived from 3,5-bis(triflouromethyl)aniline and salicylaldehyde, J. Mol. Struct. 1094 (2015) 148–160.

[41] S.M. El-Medani, A.A. Makhlouf, H. Moustafa, M.A. Afifi, M. Haukka, R.M. Ramadan, Spectroscopic, crystal structural, theoretical and biological studies of phenylacetohydrazide Schiff base derivatives and their copper complexes, J. Mol. Struct. 1208 (2020) 127860.

[42] A.R. Kennedy, L.K. Conway, J.B.A. Kirkhouse, K.M. McCarney, O. Puissegur, E. Staunton, S.J. Teat, J.E. Warren, Monosulfonated azo dyes: a crystallographic study of the molecular structures of the free acid, anionic and dianionic forms, Crystals 10 (2020) 662, doi:10.3390/cryst10080662.

[43] X. Yang, D. Yuan, J. Hou, A.C. Sedgwick, S. Xu, T.D. James, L. Wang, Organic/inorganic supramolecular nano-systems based on host/guest interactions, Coord. Chem. Rev. 428 (2021) 213609.

[44] N. Raja, R. Ramesh, Y. Liu, Paramagnetic ruthenium(III) complexes bearing O,O chelating ligands: synthesis, spectra, molecular structure and electron transfer properties, Polyhedron 31 (2012) 196–201.

[45] A.A. Abdel Aziz, F.M. Elantabli, H. Moustafa, S.M. El-Medani, Spectroscopic, DNA binding ability, biological activity, DFT calculations and non linear optical properties (NLO) of novel Co(II), Cu(II), Zn(II), Cd(II) and Hg(II) complexes with ONS Schiff base, J. Mol. Struct. 1141 (2017) 563–576.

[46] A.A. Aly, Ethyl {4-[2-(saccharin-2-yl) acetylsulfamoyl] phenylazo} cyanoacetate in the synthesis of polyfunctionally heteroaromatic derivatives, J. Heterocycl. Chem. 46 (2009) 895–902.

[47] M.M.H. Khalil, M.M. Aboaly, R.M. Ramadan, Spectroscopic and electrochemical studies of ruthenium and osmium complexes of salicylideneimine-2-thiophenol Schiff base, Spectrochim. Acta Part A 61 (2005) 157–161.

[48] M.E. Azab, M.M. Youssef, E.A. El-Bordany, Synthesis and antibacterial evaluation of novel heterocyclic compounds containing a sulfonamido moiety, Molecules 18 (2013) 832–844.

[49] R.M. Ramadan, M.S.A. Hamza, A.S. Attia, A novel structure arrangement of molybdenum dimethylglyoxime complexes; Compounds with $MoON_2C_2$ six-membered rings, Polyhedron 16 (1997) 229–233.

[50] K. Sharma, R. Singh, N. Fahmi, R.V. Singh, Microwave assisted synthesis, characterization and biological evaluation of palladium and platinum complexes with azomethines, Spectrochim. Acta Part A 75 (2010) 422–427.

[51] K. Mahajan, M. Swami, R.V. Singh, Microwave synthesis, spectral studies, antimicrobial approach, and coordination behavior of antimony (III) and bismuth (III) compounds with benzothiazoline, Russ. J. Coord. Chem. 35 (2009) 179–185.

[52] B.M. Trost, C.J. Li, Handbook of Green Chemistry, Wiley-VCH Verlag GmbH & Co, KGaA, Weinheim, 2012 Ed..

[53] C.R. McElroy, A. Constantinou, L.C. Jones, L. Summerton, J.H. Clark, Towards a holistic approach to metrics for the 21st century pharmaceutical industry, Green Chem. 17 (2015) 3111–3121.

[54] D.W. Deamer, A. Kleinzeller, D.M. Fambrough, Membrane Permeability: 100 Years since Ernest Overton, Current Topics in Membranes, 48, Academic Press, San Diego, CA, 1999.

[55] M.W. Harrold, R.M. Zavod, Basic Concepts in Medicinal Chemistry, American Society for Health-System Pharmacists, 2013.

[56] N.T. Abdel Ghani, A.M Mansour, Structural and *in vitro* cytotoxicity studies on 1H-Benzimidazol-2-ylmethyl-N-Phenyl amine and its Pd(II) and Pt(II) complexes, Spectrochim. Acta Part A 81 (2011) 529–543.
[57] R.M. Ramadan, A.F.H. Noureldeen, M.M. Abo-Aly, S.M. El-Medani, Spectroscopic, DFT analysis, antimicrobial and cytotoxicity studies of three gold(III) complexes, Inorg. Nano Met. Chem. (2021), doi:10.1080/24701556.2021.1891102.
[58] V.S. Bollu, T. Bathini, A.K. Barui, A. Roy, N.C. Ragi, S. Maloth, P. Sripadi, B. Sreedhar, P. Nagababub, C.R. Patra, Design of DNA intercalators based copper(II) complexes, investigation of their potential anti-cancer activity and sub-chronic toxicity, Mater. Sci. Eng. C (05) (2019) 110079.
[59] N. Cutillas, G.S. Yellol, C. de Haro, C. Vicente, V. Rodriguez, J. Ruiz, Anticancer cyclometalated complexes of platinum group metals and gold, Coord. Chem. Rev. 257 (2013) 2784–2797.